NAVAL POSTGRADUATE SCHOOL
Monterey, California

THESIS

ESTIMATION OF STRATOCUMULUS-TOPPED BOUNDARY LAYER DEPTH USING SEA SURFACE AND REMOTELY SENSED CLOUD-TOP TEMPERATURES

by

Marvin B. McBride III

June 2000

Thesis Advisor: Philip A. Durkee
Co-Advisor: Carlyle H. Wash

Approved for public release; distribution is unlimited

REPORT DOCUMENTATION PAGE			Form Approved OMB No. 0704-0188
Public reporting burden for this collection of information is estimated to average 1 hour per response, including the time for reviewing instruction, searching existing data sources, gathering and maintaining the data needed, and completing and reviewing the collection of information. Send comments regarding this burden estimate or any other aspect of this collection of information, including suggestions for reducing this burden, to Washington headquarters Services, Directorate for Information Operations and Reports, 1215 Jefferson Davis Highway, Suite 1204, Arlington, VA 22202-4302, and to the Office of Management and Budget, Paperwork Reduction Project (0704-0188) Washington DC 20503.			
1. AGENCY USE ONLY *(Leave blank)*	**2. REPORT DATE** June 2000	**3. REPORT TYPE AND DATES COVERED** Master's Thesis	
4. TITLE AND SUBTITLE: Title (Mix case letters) Estimation of Stratocumulus-Topped Boundary Layer Depth Using Sea Surface and Remotely Sensed Cloud-Top Temperatures			**5. FUNDING NUMBERS**
6. AUTHOR(S) Marvin B. McBride III			
7. PERFORMING ORGANIZATION NAME(S) AND ADDRESS(ES) Naval Postgraduate School Monterey, CA 93943-5000			**8. PERFORMING ORGANIZATION REPORT NUMBER**
9. SPONSORING / MONITORING AGENCY NAME(S) AND ADDRESS(ES) N/A			**10. SPONSORING / MONITORING AGENCY REPORT NUMBER**
11. SUPPLEMENTARY NOTES The views expressed in this thesis are those of the author and do not reflect the official policy or position of the Department of Defense or the U.S. Government.			
12a. DISTRIBUTION / AVAILABILITY STATEMENT Approved for public release; distribution is unlimited			**12b. DISTRIBUTION CODE**

ABSTRACT ***(maximum 200 words)***

The depth of the marine atmospheric boundary layer (MABL) is an important parameter for both scientific and operational meteorological applications. The depth of the marine boundary layer has a significant influence on the atmospheric dynamics in the coastal zone. Knowledge of the depth of stratocumulus-topped boundary layers (STBLs) will enable coastal operations to more accurately anticipate weather, and electromagnetic propagation conditions. This study develops a satellite remote sensing technique for determining the height of MABLs topped with stratocumulus clouds.

Validation of the technique using coastal rawinsonde dataset from the Monterey Area Ship Track (MAST) experiment revealed that an assumption of 41% cloud with a moist lapse rate equal to –7.0°C/km had the best overall fit to the data. However, for shallow boundary layers with depths below 400m the most accurate assumption was 75% cloud with a moist lapse rate equal to –6.5°C/km. The application of this technique to sounding data returned an overall BL depth accuracy of 50m while the satellite application returned an overall accuracy of 65m. A sensitivity analysis of both surface and cloud-top temperature revealed that a 1/2°C change in either temperature resulted in an error of 60-70m in boundary layer depth.

14. SUBJECT TERMS boundary layer depth, remote sensing, stratocumulus, AVHRR			**15. NUMBER OF PAGES**
			16. PRICE CODE
17. SECURITY CLASSIFICATION OF REPORT Unclassified	**18. SECURITY CLASSIFICATION OF THIS PAGE** Unclassified	**19. SECURITY CLASSIFICATION OF ABSTRACT** Unclassified	**20. LIMITATION OF ABSTRACT** UL

NSN 7540-01-280-5500

Standard Form 298 (Rev. 2-89)
Prescribed by ANSI Std. 239-18

THIS PAGE INTENTIONALLY LEFT BLANK

Approved for public release; distribution is unlimited

ESTIMATION OF STRATOCUMULUS-TOPPED BOUNDARY LAYER DEPTH USING SEA SURFACE AND REMOTELY SENSED CLOUD-TOP TEMPERATURES

Marvin B. McBride III
Lieutenant, United States Navy
B.S., Stephen F. Austin State University, 1993

Submitted in partial fulfillment of the
requirements for the degree of

MASTER OF SCIENCE IN METEOROLOGY AND PHYSICAL OCEANOGRAPHY

from the

NAVAL POSTGRADUATE SCHOOL
June 2000

Author: Marvin B McBride III
Marvin B. McBride III

Approved by:
Philip A. Durkee, Thesis Advisor

for C H Wash
Carlyle H. Wash, Co-Advisor

Robert L. Haney, Chairman
Department of Meteorology

THIS PAGE INTENTIONALLY LEFT BLANK

ABSTRACT

The depth of the marine atmospheric boundary layer (MABL) is an important parameter for both scientific and operational meteorological applications. The depth of the marine boundary layer has a significant influence on the atmospheric dynamics in the coastal zone. Knowledge of the depth of stratocumulus-topped boundary layers (STBLs) will enable coastal operations to more accurately anticipate weather, and electromagnetic propagation conditions. This study develops a satellite remote sensing technique for determining the height of MABLs topped with stratocumulus clouds.

Validation of the technique using coastal rawinsonde dataset from the Monterey Area Ship Track (MAST) experiment revealed that an assumption of 41% cloud with a moist lapse rate equal to –7.0°C/km had the best overall fit to the data. However, for shallow boundary layers with depths below 400m the most accurate assumption was 75% cloud with a moist lapse rate equal to –6.5°C/km. The application of this technique to sounding data returned an overall BL depth accuracy of 50m while the satellite application returned an overall accuracy of 65m. A sensitivity analysis of both surface and cloud-top temperature revealed that a 1/2°C change in either temperature resulted in an error of 60-70m in boundary layer depth.

THIS PAGE INTENTIONALLY LEFT BLANK

TABLE OF CONTENTS

LIST OF FIGURES

ACKNOWLEDGMENTS

I would like to express my deepest thanks to a number of people who encouraged me by their interest and passion in this field. Dr. Carlyle Wash who helped me get this project started and who carefully reviewed this thesis while offering constructive technical and literary criticism. I am deeply indebted to Professor Philip A. Durkee whose patient assistance, brilliant insights and wise counsel have been invaluable throughout the course of this research. He has been a great inspiration to me. Special thanks goes to Kurt E. Neilson and Mary S. Jordan whose friendship and programming skills have been instrumental in the completion of this task. Last but not least I would like to thank my lovely wife Terri and beautiful daughters Kelley and Molly whose love and support have made my experience here on that I will never forget.

THIS PAGE INTENTIONALLY LEFT BLANK

I. INTRODUCTION

The depth of the marine atmospheric boundary layer (MABL) is an important parameter for both scientific and operational meteorological applications. The depth of the marine boundary layer has a significant influence on the atmospheric dynamics in the coastal zone. Since the MABL is often topped by stratocumulus clouds, knowledge of the depth of stratocumulus-topped boundary layers (STBLs) will enable coastal operations to more accurately anticipate weather, and electromagnetic propagation conditions. A satellite remote sensing technique for determining the height of MABLs topped with stratocumulus clouds is developed in this thesis.

A. APPLICATION OF BOUNDARY LAYER DEPTH DATA

The value of knowing boundary layer height can be seen when considering propagation conditions of surface based radar platforms. Even without complete knowledge of ducting profile shapes in the region knowledge of boundary layer height is important using the assumption that the boundary layer is well mixed. Boundary layer (BL) height is directly related to the base of the trapping layer associated with atmospheric ducts that can enhance the propagation of electromagnetic (EM) energy. The base of the trapping layer is referred to as the "optimum-coupling layer". When conditions are such that the atmosphere acts as a wave-guide or duct, the propagation of EM waves is confined to a narrow region. Operational sensors that detect radar waves and other EM energy can operate more effectively when favorable ducting conditions are present.

Surface vessels can experience enhanced EM detection conditions in the presence of surface-based ducts. The "optimum-coupling layer", which is equivalent to the height of the well-mixed portion of the MABL, is related to the type of duct present. Figure 1-1 illustrates the height difference for a surface-based duct (Z_1) and for an elevated duct (Z_2). The surface-based duct normally has a lower optimum-coupling layer (Davidson, 2000). The contrast between the two types of ducts and their impact on EM propagation conditions can be seen in Figure 1-2 which shows greater detection ranges for surface-based ducts vice elevated ducts (Rogers, L.T., 1999).

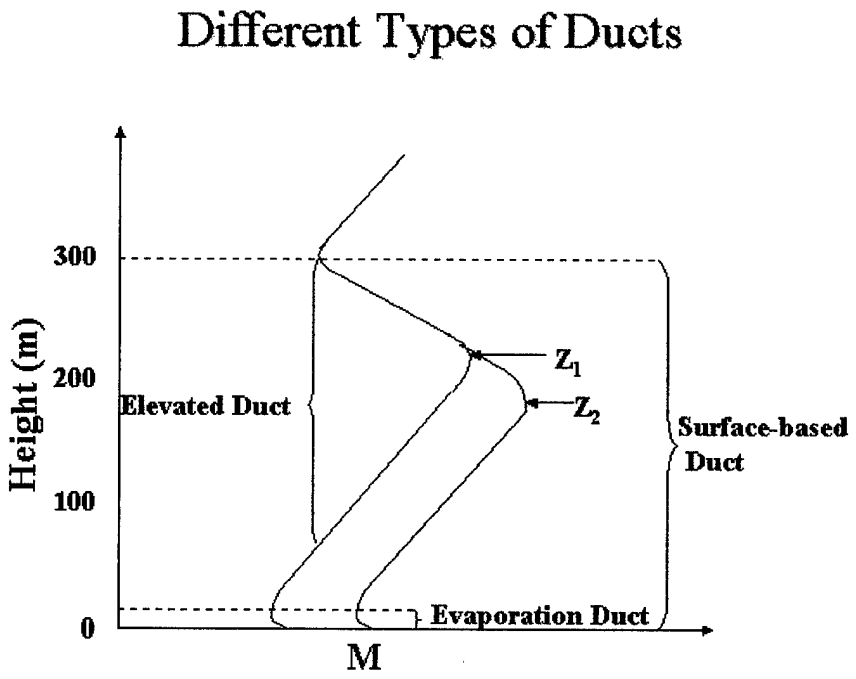

Figure 1-1: Examples of elevated and surface-based ducting conditions.

Different types of ducting

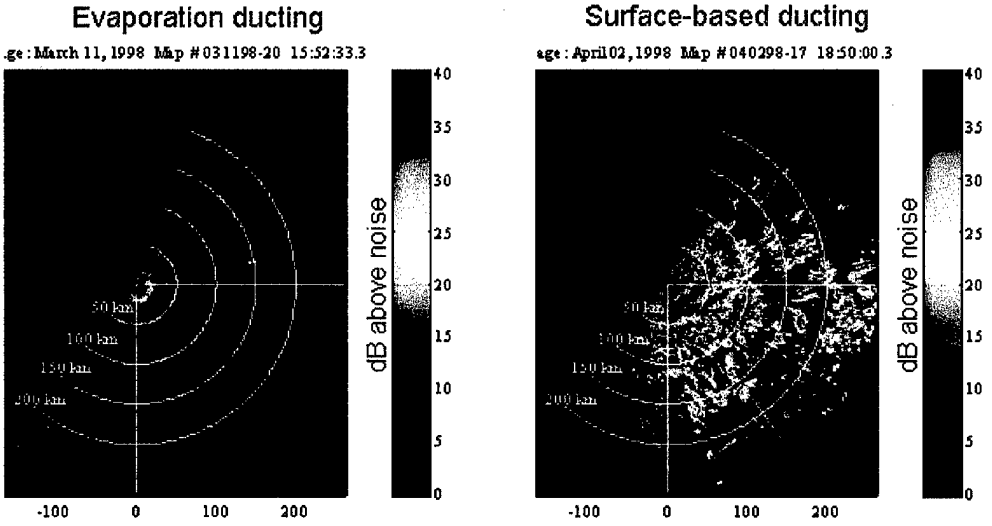

Figure 1-2: Radar image of elevated and surface-based ducting conditions.

While boundary layer depth information is of critical importance for determining the type and effect of ducting conditions, the moisture content above the BL must also be know in order to determine if a trapping layer occurs, i.e., to determine the shape of the refractivity (M) profile. Due to the presence of strong subsidence the air above the BL is generally very dry. Figure 1-3 shows a sounding from the Arabian Gulf, which clearly shows the dry nature of the atmosphere above the boundary layer in the presence of subsidence (Davidson, 2000). Ducting conditions are very common especially over eastern ocean basins where strong subsidence from a semi-permanent high is common. Figure 1-4 shows the importance of the knowledge and application of boundary layer depth to the determination of ducting

conditions can be seen when considering the prevalence of ducting conditions around the world. (Ortenburger et al, 1985)

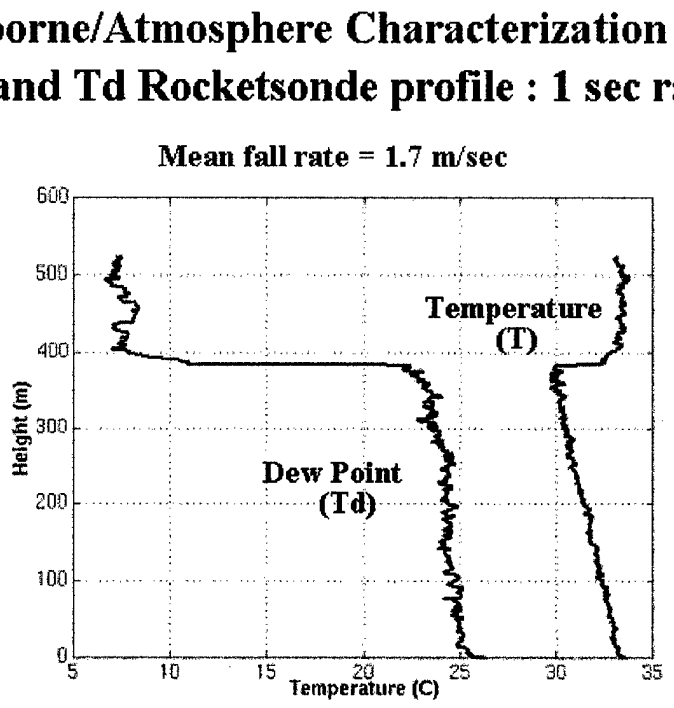

Figure 1-3: Example of the nature of moisture profiles in and above the BL ducting in a region of strong subsidence.

Rosenthal et al, [1997] showed that it is possible to obtain a statistical correlation of duct height (BL height) with cloud-top temperature (T_{CT}) off the coast of California to within approximately 133m of accuracy 80% of the time (Rosenthal, J.S., 2000). The correlation of T_{CT} to duct height implies that a remote sensing

technique for determining BL depth under strong subsidence inversions would provide accurate, real-time estimation of ducting conditions.

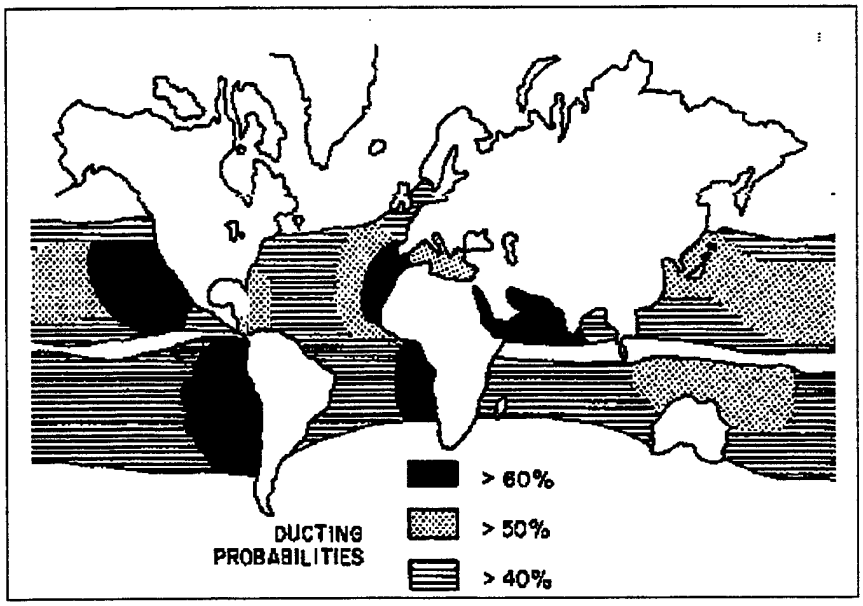

Figure 1-4: World wide frequency of ducting occurrence. (from Ortenburger, L.N., et al, 1985)

B. METHODS OF CLOUD HEIGHT DETERMINATION

Direct measurements of boundary layer height are often difficult and impractical to make and are therefore relatively rare. This has led to the development of several methods by which the height of the MABL may be directly and indirectly determined in cloudy and in cloud free atmospheres. In the past techniques for determining the height of the MABL were limited to land and ship launched radiosondes. However, several techniques have been developed to accomplish the same goal in a more efficient manner. Some examples

of these techniques include ground-based SOund Detection And Ranging (SODAR) (Gaynor and Mandics, 1978) and LIght Detection and Ranging (LIDAR) (Eloranta et al., 1975). These techniques require multiple stations and even in optimal circumstances they fail to provide a complete view of the marine boundary layer due to their limited spatial extent.

The development of satellite-derived retrieval methods provides an expanded observation area and therefore a more complete picture of boundary layer depth. Many satellite techniques exist for measuring boundary layer properties including multispectral techniques for cloud free boundary layers (Kren, 1987). This study will focus on cloudy boundary layers since, as Kuze and Chance [1994] have shown, clouds cover more than 50% of the Earth's surface.

There are several types of cloud height retrieval methods that utilize satellite data. These techniques can be broken up into two general categories. The first group extracts cloud top height in a direct way from satellite measurements including stereoscopic analysis and cloud shadow measurements. Stereoscopic analysis uses offset image pairs that are correlated to give a horizontal shift that is turned into a cloud top height. However, this technique is only applicable when near-coincident satellite image pairs are available for comparison and is therefore restricted to geostationary imagery (Shenk et al., 1975). Cloud shadow measurements use the given solar and satellite geometry to calculate cloud height from the length and direction of observed cloud shadows. This technique applies only to clouds with limited vertical (Hasler et al., 1991).

The second category uses the physical characteristics of the atmosphere to model cloud height. Some of these techniques include the use of atmospheric absorption bands (CO_2 or O_2), and bispectral estimations. Atmospheric absorption techniques use model optical path length and therefore height from within an absorbing region of the electromagnetic spectrum. Typical meteorological satellites such as the Advanced Very High Resolution Radiometer (AVHRR) instrument on the NOAA polar orbiters employs neither the correct wavelength regions nor the narrow bandwidths needed to estimate cloud top height. Bispectral methods on the other hand derive cloud-top height by comparing cloud-top brightness temperature (T_B) with satellite derived vertical soundings such as from the Tiros Operational Vertical Sounder (TOVS). Unfortunately, satellite soundings lack the vertical resolution that is necessary for accurate estimations of STBL cloud height. Another option is to compare T_B with sounding output from numerical weather model temperature fields. These types of fields nominally have temperature errors of 1-2°C and this type of application generally yields cloud height errors of 300-500 meters (Simpson, et al, 2000).

The use of satellite data for broad spatial measurements of the depth of the STBL has the potential to significantly improve the understanding of large-scale STBL properties and dynamics. This study will present and test a technique for estimating the depth of the STBL by using a vertical thermodynamic model that calculates boundary layer depth from independent measurements of sea surface temperature (T_S) and satellite derived cloud-top brightness temperature.

In Chapter II of this study the theoretical background behind the structure and dynamics of the STBL as well as the theory behind satellite derived cloud-top brightness temperatures will be presented. Chapter III will present the datasets utilized in this study as well as the specifics of the retrieval technique. Chapter IV will present the pertinent assumptions needed to accurately estimate the depth of the STBL and the results of the technique applied to atmospheric soundings and satellite derived T_B. Chapter V covers the conclusions drawn from this thesis research and recommendations for further study.

II. BACKGROUND

With the proper assumptions, it is possible to indirectly determine the depth of the STBL using sea surface temperature and satellite derived cloud-top brightness temperature. The technique requires brightness temperatures from AVHRR channel 4 (11μm wavelength), and an assumption of vertical cloud fraction in order to determine the height of transition from the dry to moist (pseudo-adiabatic) lapse rate within the STBL. This chapter covers the structure and dynamics of cloudy marine boundary layers, and the basic radiative transfer process that determines the measurement of cloud-top brightness temperature.

A. LAPSE RATES IN THE STBL

The Earth's atmosphere cools with increasing height due to the fact that it is heated primarily from below by longwave radiation emitted from the Earth. The rate of cooling is known as the lapse rate of the atmosphere. The lapse rate of the atmosphere is associated with the mathematical slope of the line of temperature vs. altitude. By convention a decrease of temperature for increasing altitude is denoted as a positive lapse rate.

The technique described here assumes adiabatic lapse rates within the STBL. However, the atmosphere near the Earth's surface is adiabatic only under certain conditions. These conditions include heavy cloud cover, which limits radiative heating of the surface, and turbulence sufficient to mix the air and smooth out temperature gradients.

In other words, the atmosphere may not be adiabatic due to insufficient mixing and/or solar heating of the surface.

These two processes produce highly variable temperature behavior in the lowest layers of the atmosphere. Solar heating of the surface is most pronounced over land-covered areas. Over the ocean the high heat capacity of water prevents significant diurnal warming and cooling of the ocean surface even during cloud free days. Therefore, the STBL can be said to meet these two criteria most of the time, and an adiabatic lapse rate is therefore a good assumption.

1. Dry Adiabatic Lapse Rate

The dry adiabatic lapse rate is the rate at which air temperature decreases with increasing altitude for an air parcel that is unsaturated. The decrease in temperature is due to the adiabatic expansion (occurring without loss or gain of heat) of a parcel of air. An expanding parcel of air will cool as the volume increases due to conservation of energy. The value for the dry adiabatic lapse rate is approximately -9.8°C/km.

2. Moist Adiabatic Lapse Rate

The moist adiabatic lapse rate is the loss of temperature with increasing altitude for an air parcel that is saturated. If a saturated air parcel is adiabatically expanded, the temperature will decrease, but this decrease causes the parcel to become increasingly supersaturated. Saturation leads to condensation, and the latent heat released in this process warms the parcel. The warming from the latent heat release partially offsets the loss of temperature due to adiabatic expansion leading to a lapse rate that is smaller in magnitude than the dry adiabatic lapse rate.

It can be seen in Figure 2-1 that the pseudo-adiabatic lapse rate is a nonlinear function due to the addition of latent heat. However, this lapse rate is essentially constant below 1.5km. Since the STBL rarely exceeds 1.5km in height, a constant value is used for the pseudo-adiabatic lapse rate in this procedure. (Hsieh, 1987)

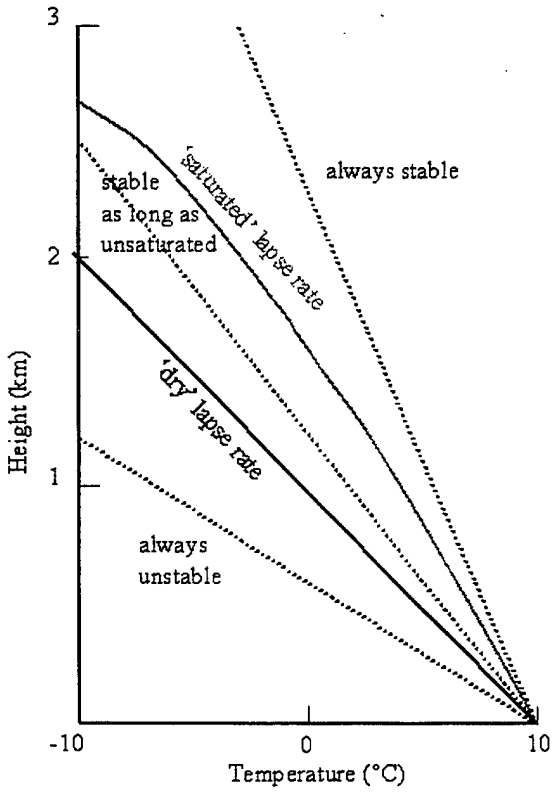

Figure 2-1: Atmospheric lapse rates.
(from Hsieh, 1987)

B. STRUCTURE OF THE STBL

For cloudless boundary layers the majority of the turbulence is produced at the surface by thermal convection and/or vertical wind shear. Surface turbulence leads to the

upward transport of momentum and moisture in the layer. In the STBL an additional source of turbulence is added by the presence of the cloud. Stratiform clouds at the top of the marine boundary layer result in dynamics that are significantly more complicated than for the cloud free boundary layer. The STBL is produced and maintained due to the balance of several processes. The nature of these processes will be discussed in the following sections.

1. Cloud-Top Inversion

STBLs form under inversion layers that are due to the descending, or subsiding air in the atmosphere associated with high-pressure areas. The inversion layer itself is a product of the adiabatic heating of the descending air and the layer just above the subsidence inversion is usually dry. Within an inversion layer there is a reversal of the normal lapse rate where temperature increases with altitude. The STBL is most prevalent beneath strong subsidence inversions over subtropical oceans. These areas include eastern subtropical ocean basins and mid to high latitude oceans where marine stratiform clouds are common. Specifically, the area in the North Pacific Ocean off the California coast is typically covered with marine stratocumulus clouds during the summer months when the region is dominated by a persistent sub-tropical high pressure system.

The degree of turbulent mixing within the boundary layer determines the distribution of moisture, which influences the thickness of the cloud and can change the overall depth of the boundary layer. The following is a breakdown of the processes that produce the mixing required to maintain stratocumulus clouds. (Stull, 1988)

Surface-based Free Convection: Free convection occurs when cold air is advected over a warmer surface since the condition of cold air over warm water results in an unstable atmosphere. The maintenance of stratocumulus clouds and fog off the coast of southern California is strongly influenced by surface-based free convection.

Shear-generated Mechanical Turbulence: Shear turbulence is associated with strong BL winds that can cause convection (mixing) that is sufficiently strong enough to mix the moisture from the ocean surface to the cloud layer. The efficient redistribution of surface properties caused by mixing is an important factor in the maintenance of marine stratocumulus clouds.

Cloud-top Radiative Cooling: The radiative heat loss at the top of stratocumulus clouds is a significant factor in the maintenance of the STBL. The cooling at the tops of stratocumulus clouds creates pockets of cold air that sink and mix with lower levels and help maintain the condensation necessary to produce cloud droplets. Cloud-top cooling is a process that is important to the maintenance of stratocumulus clouds as long as there are not higher clouds that can reduce the cooling of the lower cloud deck by radiating energy down onto the cloud top.

Cloud-base Radiative Heating: The process of radiative heating, by radiation emitted from the surface and absorbed at the cloud-base, plays an important role in the destabilization of the cloud layer while stabilizing the subcloud layer.

However, it is generally much weaker than cloud-top cooling due to the smaller temperature difference between layers.

Cloud-layer Shear: Shear generated in the cloud-layer generally produces mechanical turbulence and mixing near the top of the cloud. The turbulence resulting from cloud-layer shear produces small scale entrainment mixing that can decouple the cloud unless there are other turbulent processes present to more evenly distribute moisture and temperature throughout the BL.

2. Cloud Base or LCL

The altitude at which saturation occurs inside an air parcel, as it rises, expands and cools, is called the lifting condensation level (LCL). The LCL corresponds to the base of the clouds in the STBL. The value of the LCL is not constant in the STBL and its variation is governed by the degree of mixing or turbulence within the boundary layer and by a destructive process known as decoupling.

Decoupling is the process by which stratocumulus clouds become disconnected from the lower regions of the marine boundary layer. When the boundary layer is decoupled a small inversion develops below the cloud base, which inhibits mixing from the ocean surface to the cloud and creates a lower, moist layer beneath a drier, cloud mixed layer. Decoupling occurs as a result of two primary processes in the boundary layer (Tjernström, 1998).

a. Decoupling by Solar Absorption (Diurnal Decoupling)

The process of diurnal decoupling is caused by variations in mixing due to cloud-top radiative cooling. During both day and night the longwave radiation that is

emitted upward from the cloud top is generally higher than the incoming energy received from the dry above the cloud. The net loss of radiative energy causes an imbalance that cools the top of the cloud layer and leads to thermally induced instability since the top of the cloud is now cooler than the bottom. The instability is enhanced under daytime heating as shortwave solar radiation penetrates into the cloud which warms it from within.

The effect of solar radiation can cause a secondary inversion to form at the cloud base if the surface flux is weak. The secondary inversion separates the cloud from the surface and a second turbulent layer forms in the STBL. The diurnal fluctuation of cloud thickness due to this process plays an important role in the understanding of the dynamics of the STBL.

b. Decoupling Due to Precipitation

The second decoupling process is due to precipitation out the bottom of the cloud. As described above, vertical cooling rate of the atmosphere is modified by the release of latent heat as water vapor condenses. However, as drizzle falls out of the cloud some of it evaporates in the air below leading to a cooler, moister sub-cloud layer. The development of a sub-cloud layer causes a stable layer to form near the cloud base that prevents the boundary layer from being well mixed.

3. The Surface (Sea and Air Temperature)

The surface air temperature (T_A) and sea surface temperature (T_S) are usually close in magnitude. If a gradient in temperature occurs, fluxes develop which produce

differences in T_A and T_S such that they seldom precisely equal in value. There are several physical process which can affect the differences in T_A and T_S. These processes include:

Convection: Convection is a process by which heat is transferred due to the physical movement of air. Convective processes help to minimize temperature fluctuations by vertically mixing the air near the surface.

Conduction: The transfer of heat through matter by communication of kinetic energy from particle to particle is known as conduction. Air is made up of many dispersed molecules that inhibit the process of conduction making air an effective insulator. The process of conduction is negligible when compared to the other process in the atmosphere, which are much larger in magnitude.

Radiation: Radiation is the transfer of heat via electro-magnetic energy which is transferred to the atmosphere through absorption by gaseous constituents such as water vapor and carbon dioxide. Radiation from the ocean has a very strong moderating effect on the air temperature over the ocean's surface, which is due to the large heat capacity of the ocean. The high heat capacity of the ocean enables it to gain and lose energy without large changes in T_S.

Advection: In many cases, advection is the most influential of the four processes in amplifying the sea/air temperature difference. When an air mass moves out of its generation area and moves over ocean waters with different properties, strong fluxes of temperature and moisture result. These fluxes act to reduce the difference between the sea surface and the surface air temperature.

Klein and Hartmann [1993] showed the annual, climatological cycle of T_S and T_A difference to be very small in the Californian stratus region. Figure 2-2 shows the difference between T_A and T_S is typically between 0.5°C and 1°C. This was done when they compared the seasonal variation of stratus cloud amounts off the coast of California using shipboard data. It is therefore assumed that the difference between the air and sea surface temperature is nominally within 1°C at any given time. This small (1°C) temperature difference is primarily due to climatologically weak surface fluxes of sensible heat. For simplicity in this study, it is initially assumed here that the sea surface temperature is equal to the surface air temperature.

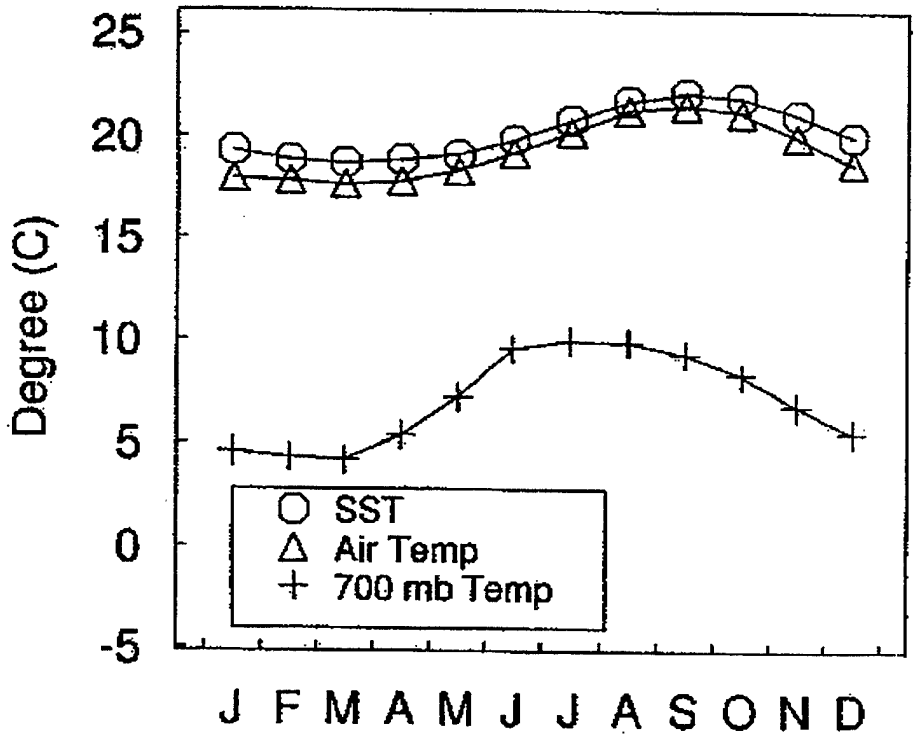

Figure 2-2: The annual cycle of T_S and T_A difference.
(Klein and Hartmann, 1993)

C. SATELLITE DETERMINED CLOUD-TOP TEMPERATURE

The technique presented in this thesis uses the AVHRR sensor to determine cloud-top temperature. AVHRR channel 4 measures radiance at 11μm wavelength. Channel 4 is ideal for measuring surface or cloud-top radiance due to the lack of gaseous absorption in the atmosphere at this wavelength. (Kidder and Vonder Haar, 1995)

1. Radiative Transfer to Determine Cloud-Top Temperature

It is assumed that the cloud layer being sensed is thick and that the atmosphere above the cloud top is dry. From Schwartzchild's equation the radiance at the top of the atmosphere is:

$$L_t(\lambda,\theta,\varphi) = \varepsilon_s(\lambda,\theta)B(\lambda,T_s)\tau_d(\lambda) + \int_{p_0}^{0} B(\lambda,T(p))\frac{d\tau_d(\lambda,p)}{dp}dp \qquad (2\text{-}1)$$

where L_t is the spectral radiance at the top of the atmosphere as a function of wavelength (λ) and direction (θ,φ). $\varepsilon_s(\lambda,\theta)B(\lambda,T_s)\tau_d(\lambda)$ is the emitted radiance from the surface as a function of wavelength and surface temperature. $\tau_d(\lambda)$ is the total direct transmittance throughout the full extent of the atmosphere as a function of wavelength and $\tau_d(\lambda,p)$ is the direct transmittance from pressure p to the top of the atmosphere (p=0). $B(\lambda,T(p))$ is the Planck blackbody emittance as a function of wavelength, and temperature at a given pressure. The derivative of the direct transmittance (τ_d) with respect to pressure is a weighting function that determines the contribution to L_t due to at each vertical position in the atmosphere.

For the STBL $[d\tau_d(\lambda,p)/dp]dp = 1$ over a few meter thick layer thick near the cloud top. Therefore, nearly all of the radiance emitted from the cloud comes from the upper portion only. The surface term $[\varepsilon_s(\lambda,T_s)\,\tau_d(\lambda)]$ goes to zero since the cloud is opaque at these wavelengths and it absorbs all of the energy from the surface. The final result is:

$$L_t = B(\lambda, T_{CT}) \tag{2-2}$$

Here L_t is measured by the sensor at λ and the value of T_{CT} can be readily determined from inversion of the Planck blackbody relation.

2. Errors in Satellite Determined T_{CT} of the STBL

Several conditions can potentially interfere with the determination of T_{CT} from satellite T_B.

a. High Clouds

The presence of higher clouds (e.g., cirrus) above the STBL produces lower values of T_{CT} due to the lower emitted radiance of clouds that exist in the higher, colder levels of the atmosphere. The presence of cirrus clouds in particular can be a problem due to the fact that cirrus clouds are often thin and difficult to detect without multispectral techniques. Therefore, the presence of cirrus clouds in the vicinity of the STBL can introduce significant errors in low level, satellite derived cloud-top temperatures.

b. Limb Darkening

When a measurement is taken from a satellite at the periphery of its field of view the radiance that is detected must pass through a larger volume of atmosphere than radiance measured from nadir. The effect of greater atmospheric interaction reduces the amount of cloud-top radiance that reaches the satellite sensor. The AVHRR sensor has a scan angle from nadir of +/-55.3° (Kidder and Vonder Haar, 1995). Measurements made at an angle of 55.3° are not only made through an increased atmospheric volume but radiance emitted from the cloud-top has an angular dependence as well. The radiance emitted from a cloud decreases as the view angle increases. Therefore measurements of T_{CT} made at the edge of a satellite pass are often significantly reduced in radiance.

D. THE VALIDITY OF A WELL-MIXED STBL

Within the STBL the potential temperature and water vapor mixing ratio are homogeneous due to turbulent mixing within the layer. The eddies which produce this mixing are due to the presence of buoyancy and shear effects. The magnitude of buoyancy production within the STBL is small due to the high heat capacity of the ocean which prevents large diurnal temperature fluctuations. Nighttime radiative cooling of the sea surface prevents the establishment of a near surface stable layer. Therefore, the STBL is often neutrally stable with only slight diurnal variations. (Kren, 1987)

The weakly unstable or neutral STBL is influenced by wind shear as well. The effect of wind shear on the STBL is to produce turbulent eddies which mix the STBL. Turbulence produced by both buoyancy and shear is generally sufficient to mix the STBL.

Some regions under synoptically induced subsidence inversions have a stable STBL where mixing is often suppressed. These areas have relatively cold sea surface temperatures that often comes from the coastal upwelling found along the west coast of continents. In these areas where the STBL is not well mixed, using a dry adiabatic lapse rate will add uncertainty to the final value of boundary layer depth. The accuracy of the technique used in this thesis under these conditions will be described in the next few chapters of this text.

The technique presented in this thesis has certain limitations which constrain its applicability. The technique requires knowledge of the temperature of both the sea surface and the cloud-top. However, satellite techniques for obtaining sea-surface temperature require a cloud-free atmosphere, and techniques for obtaining cloud-top temperature requires either an atmosphere with little water vapor above the STBL, or knowledge of the water vapor content so its effects can be corrected. The technique presented here has potential application in regions of strong subsidence inversions where cloudy boundary layers persist. Sea surface temperature data can be provided by ship observations, recent satellite analyses of SST from clear sky periods or predictive ocean models.

THIS PAGE INTENTIONALLY LEFT BLANK

III. DATA AND METHODOLOGY

A. MONTEREY AREA SHIP TRACK (MAST) EXPERIMENT DATASET

The primary data set for this thesis comes from the Monterey Area Ship Track Experiment (MAST) (Durkee et al, 2000). MAST was a multi-agency effort designed to determine the physical nature of ship tracks via the collection of sounding, aircraft and satellite data off the coast of Central California. Figure 3-1 depicts the MAST operating area. This thesis will focus on AVHRR satellite data and radiosonde data collected by the R/V *Glorita* during the MAST experiment.

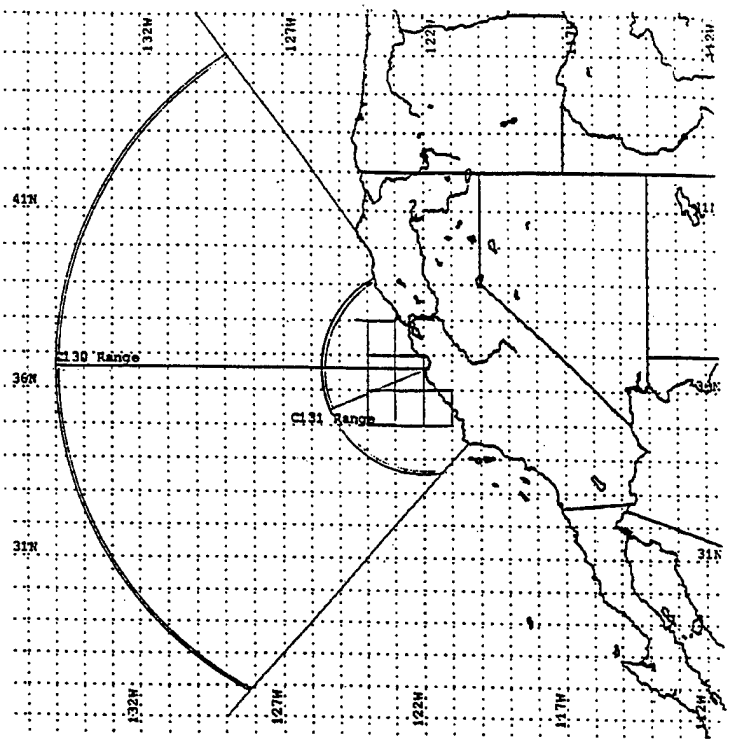

Figure 3-1: MAST Experiment 1994 Operations Area.

1. Radiosonde Data

The R/V *Glorita* launched an average of six radiosondes a day at intervals of roughly four hours for a total of 94 radiosonde soundings (designated GL01-GL94). Parameters measured with the radiosondes were pressure, temperature and relative humidity. These measured quantities where then used to derive values for height, dewpoint and mixing ratio. The techniques used to derive these quantities are included in Appendix B.

2. Surface Observation Data

Personnel onboard the R/V *Glorita* made hourly measurements of sea surface temperature (T_S), air temperature (T_A), relative humidity, as well as wind speed and direction. However, gaps in T_S measurements did occur when the temperature sensor was not in the water. Additionally these measurements are amplified by general comments on sky conditions made during radiosonde launch times.

3. Satellite (AVHRR) Data

Imagery from AVHRR Channels 1-5 of the NOAA-9, 10, 11, and 12 satellites was recorded during the experiment. Channel 4 (11μm) brightness temperatures from this imagery were used to determine the cloud top temperature at the location of a given sounding from the R/V *Glorita*.

B. ANALYSIS PROCEDURE

In order to determine the depth of the STBL a vertical, thermodynamic model was constructed. The model assumes that unsaturated air follows the dry adiabatic lapse rate

(Γ_d) until the LCL is reached. From the LCL to the cloud top the air is saturated and follows a pseudo or moist adiabatic lapse rate (Γ_m). With a given assumption of cloud thickness these two lapse rates can be combined in order to give a more complete thermodynamic picture of the STBL.

The combination of Γ_d and Γ_m determines a cloud-top height (Z) for a given surface temperature (T_S) and cloud-top temperature(T_{CT}). The constant lapse rate equation $\Gamma = (T_{CT}-T_S)/Z$ is simply rearranged algebraically to yield the formula for height $Z = (T_{CT}-T_S)/\Gamma$. Given a formula for height based on temperature and lapse rate only, it is now possible to compute heights based on the moist and dry adiabatic lapse rates for given values of T_{CT} and T_S.

An assumption of vertical cloud fraction must be made in order to give a proper physical parameterization of how much of the boundary layer follows Γ_m and how much follows Γ_d. Since the actual height of the boundary layer is unknown an initial value, or first guess, for the boundary layer height must be used in order to determine the LCL or cloud base height. The LCL in this technique is derived from an assumed fraction of the total, dry adiabatic height (Z_d).

Figure 3-2 shows an example where it is assumed that the upper one-third of the boundary layer is cloud and the remaining two-thirds of the boundary layer is cloud-free air. The LCL is determined by multiplying the total height of the cloud-free boundary layer (obtained via the dry adiabatic lapse rate) by two-thirds. The remainder of the boundary layer height is calculated from the LCL by using the pseudo-adiabatic lapse rate

until the value of T_{CT} is reached. However, by virtue of the fact that the pseudo-adiabatic lapse rate is steeper than the dry lapse rate this process produces a slightly larger fraction of cloud than is initially assumed. Therefore, when an assumption of $1/3^{rd}$ cloud is made based on the height of a totally dry BL, the increase in height from the moist-adiabatic lapse rate produces a final BL distribution of 41% cloud and 59% cloud-free atmosphere.

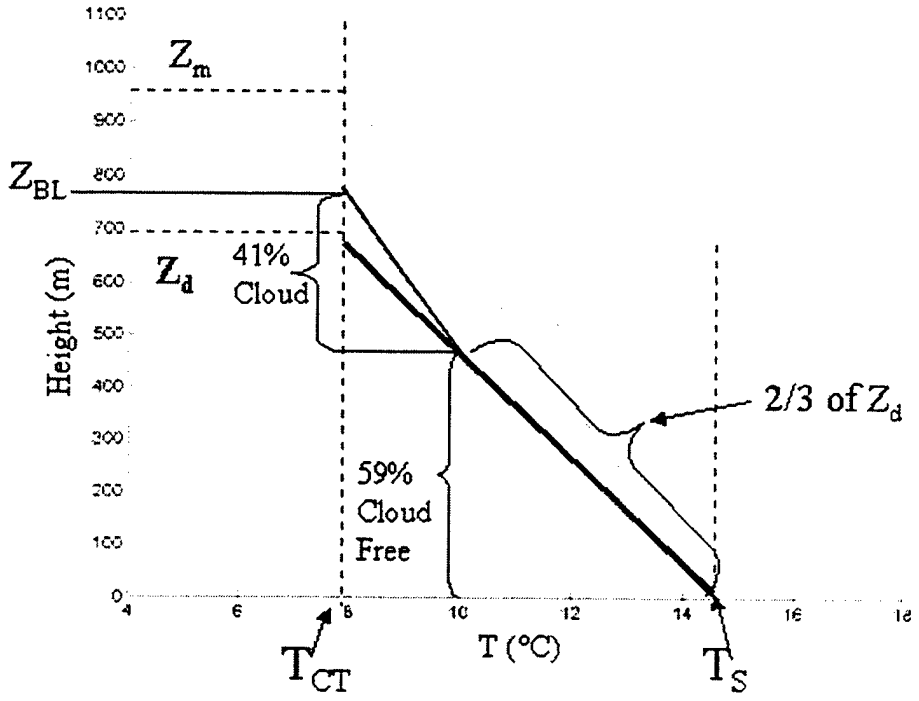

Figure 3-2: The application of the assumption of a cloud thickness of 41% and how it is derived from the dry adiabatic height Zd.

In order to calculate the height of the lower, cloud-free portion of the boundary layer the height of the entire boundary layer (i.e., from T_S to T_{CT}) must be computed along the dry adiabat with the relation $Z_d = (T_{CT}-T_S)/\Gamma_d$ where Z_d is the height of the boundary layer if it were entirely cloud free. The height of the cloud free portion of the boundary layer is then simply the height of the cloud-free BL multiplied by a slight

overestimate of the initial fraction of cloud-free STBL or $Z_{CF} = Z_d*(F_{CF})$. Where Z_{CF} denotes the initial estimate of the height of the cloud-free STBL and F_{CF} is the initial estimate of the cloud-free fraction of the STBL.

Once the initial height of the cloud free portion of the boundary layer (which is actually the height of the cloud base) is determined, the corresponding temperature at that height must be known in order to calculate the height of the saturated portion of the boundary layer. The temperature at the cloud base or LCL is computed by the relation $T_{CF} = Z_{CF}*\Gamma_d + T_S$ which then allows for the same fundamental lapse rate relation to be used in the upper two thirds of the boundary layer. This final height is combined with the height of the below cloud BL to yield the total height of the STBL via the following relation: $Z_{BL} = Z_{CF} + (T_{CT}-T_{CF})/ \Gamma_m$.

In order to determine the accuracy of the technique, values of T_A and T_{CT} were taken directly from the Glorita soundings and used to determine the height of the STBL. To determine the accuracy of the technique using satellite data, the inversion temperature from the sounding is replaced by the cloud-top brightness temperature from the AVHRR channel 4 imagery. A total of 46 soundings were used from the MAST dataset and 48 soundings were dismissed outright from the MAST dataset due to insufficient MABL clouds. See Table 3 in Appendix A for more detail on which soundings were dismissed from the dataset.

THIS PAGE INTENTIONALLY LEFT BLANK

IV. RESULTS

A. ASSUMPTIONS

Two primary assumptions must be made in order to model the general state of the STBL. The amount of cloud must be specified and the lapse rates of the atmosphere in the cloud and below cloud must be given. In the STBL it is assumed that all lapse rates are of constant value and near adiabatic in nature. The below cloud atmosphere is assumed to be exactly dry adiabatic with a lapse rate of Γ_d = -9.8°C/km and within cloud the value of the pesudo-adiabatic lapse rate is initially given the standard atmospheric value of Γ_m = -6.5°C/km.

It was initially assumed that the most common ratio of saturated to unsaturated air in the STBL was 2/3rd cloud to 1/3rd unsaturated (below cloud) air. However, results have shown that a more accurate depiction of the STBL requires an assumption of 75% cloud for shallow boundary layers (below 400m deep) and a value of 41% cloud for boundary layers deeper than 400m. Above 400m the value for the pseudo-adiabatic lapse rate was modified to a value of Γ_m = -7.0°C/km to partially compensate for its non-linear nature as altitude increases. The reasons these assumptions were chosen will be discussed below.

B. SOUNDING APPLICATION

In order to validate the physical reasoning of the technique described in Chapter III, the method was applied to the soundings from the R/V *Glorita*. The method was run

with several different values for Γ_m and cloud thickness in order to determine the best set of parameter values. The results for each set of assumptions were organized by the difference between the actual BL height and the calculated height of the STBL (denoted as ΔH). Throughout the verification process the assumptions made about the STBL were modified in order to minimize the value of ΔH

1. Actual Depth Method

The distribution of ΔH with respect to the actual BL depth was plotted in Figure 4-1, which shows how the two sets of assumptions (75% and 41% cloud) begin to diverge in the vicinity of 400 meters. Based on these criteria it was determined from the sounding results that there was a discontinuity in the accuracy of a single set of assumptions at around the 400m point. Boundary layer cases with depth less than 400m are more accurately modeled by an assumption of 75% cloud with a lapse rate of Γ_m = -6.5°C/km. These values were the only set of assumptions that returned a value for $\Delta H < 100$m in all cases below 400m. For boundary layers deeper than 400m it was determined that an assumption of 41% cloud combined with a lapse rate of Γ_m = -7.0°C/km returned the most accurate height. These assumptions for soundings above 400m produced a height differential (ΔH) that was consistently below 100m for the majority of the soundings.

Figure 4-2 shows how the two sets of assumptions were combined into a two-layer model in order to give a more accurate picture of the total STBL. The height produced by this two-layer procedure were plotted against the actual BL height with the

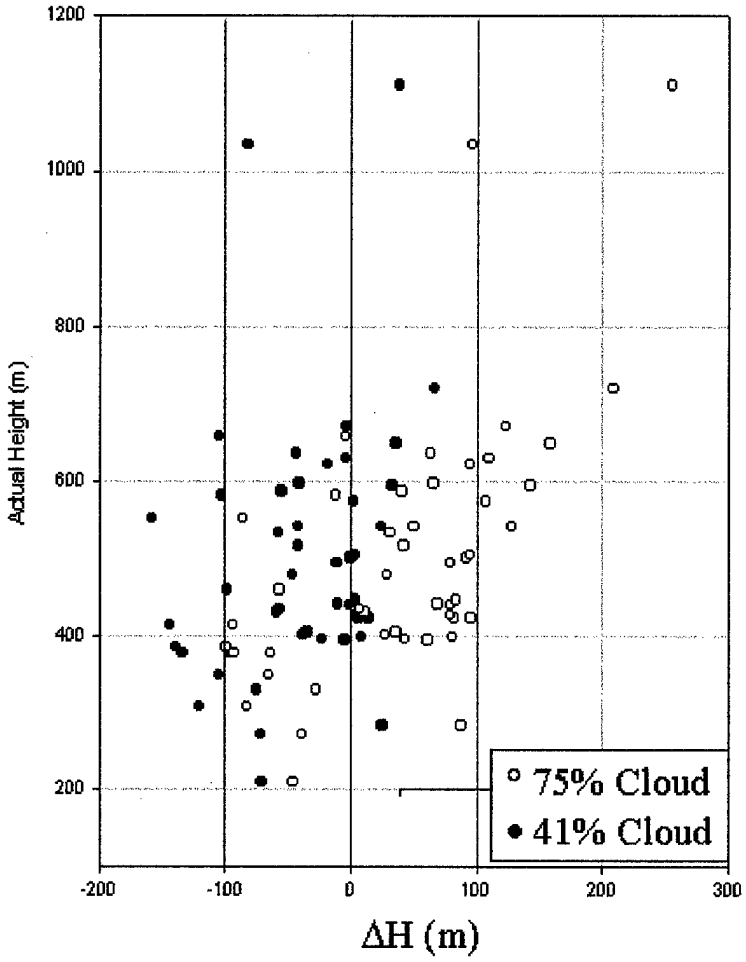

Figure 4-1: Scatter plot of the two primary sets of assumptions applied all soundings.

The results of this regression produced a line with a slope of 1.0283 where a slope of 1.0 is a perfect correlation. The line was offset from the origin by a value of -41m while the overall error of the estimate of this technique is 56m. Table 1 in Appendix A shows how several of the different assumption sets affect the determination of boundary layer height.

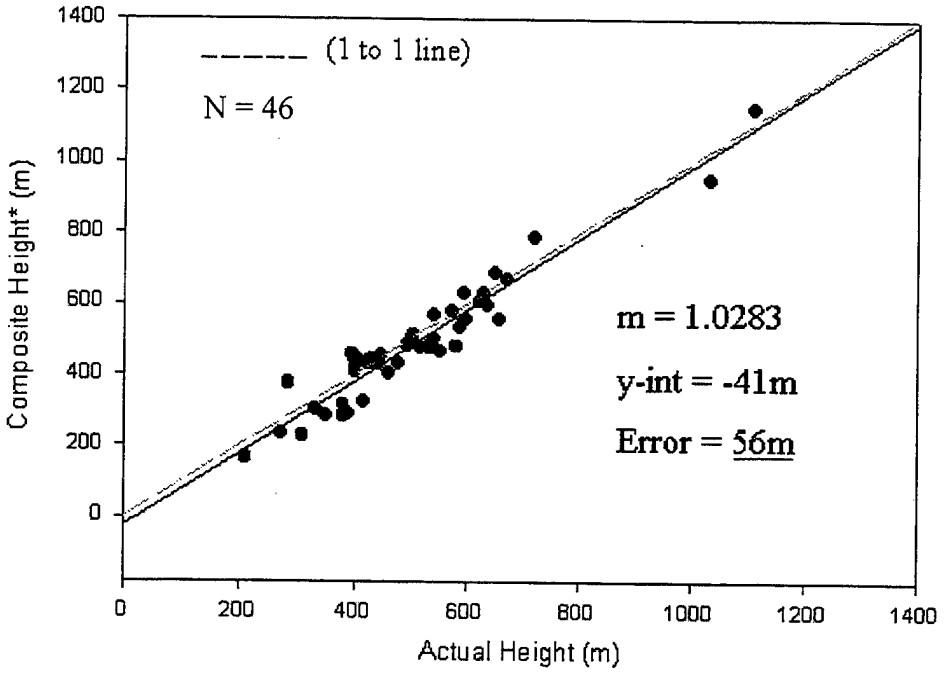

Figure 4-2: Linear regression of actual vs. calculated boundary layer height using sounding data. The solid line is the regression line and N is the number of data points.

2. First Guess Method

While this process produces favorable results it requires previous knowledge of the actual depth of the STBL. Since the actual depth of the STBL is the goal of this thesis it cannot be used experimentally to determine the dividing line between the two sets of assumptions. Therefore, a "first guess" must be made in order to determine which set of assumptions to use.

It can be seen in Table 1 that for a single set of assumptions the most accurate parameters over the entire STBL are a 41% cloud layer and pseudo-adiabatic lapse rate of Γ_m = -7.0°C/km. These assumptions were applied to the entire STBL and once an initial value of BL depth was obtained, the "shallow" set of assumptions were applied to the

soundings below the depth of 400m. Figure 4-3 shows the results from this two-step process where soundings were plotted against the actual BL depth and a linear regression was performed. The regression was found to be even more accurate than the original application of the assumptions with a slope of 1.0080, an offset of –24m and an overall error estimate of 50m.

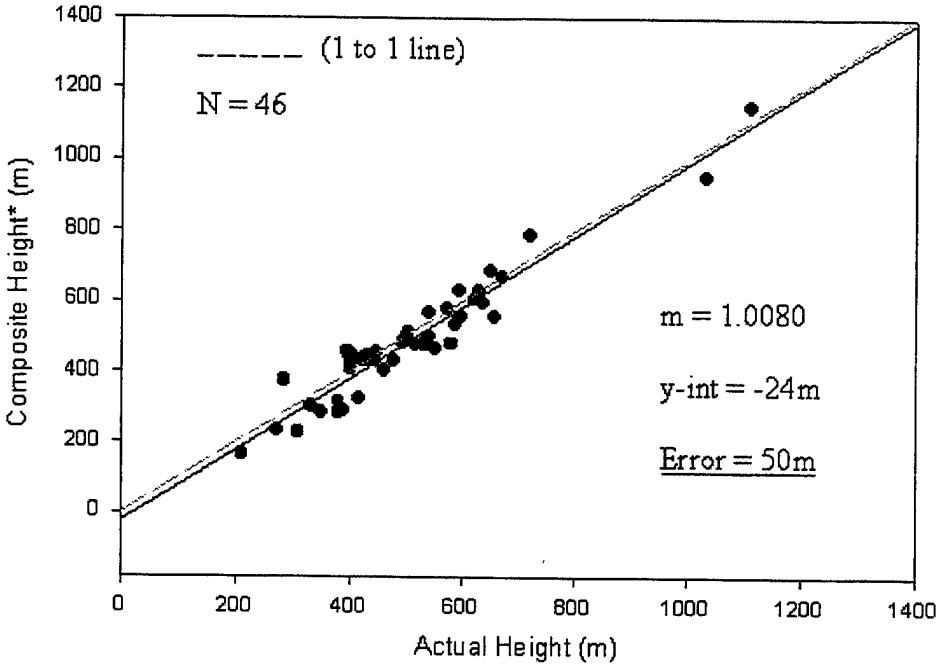

Figure 4-3: Linear regression of actual vs. calculated boundary layer height using sounding data. The solid line is the regression line and N is the number of data points.
* - Indicates the composite BL height was determined by the two-step process of the application of BL assumptions.

The soundings from the R/V *Glorita* indicate that shallow BLs, (Z_{BL} < 400m) have a larger fraction of the BL that is saturated (cloudy) air than for deeper BLs. However, the height value of 400m is by no means an absolute dividing line between BLs with differing percentages of cloud. The MAST dataset contains several cases where

soundings with BL depths above 400m contain less cloud than 75%. When the assumption of 41% cloud is applied to these cases a significant underestimate is returned. This occurs due to the fact that when the assumption of 41% cloud is applied to these cases, the predominance of the dry lapse rate produces a significant underestimate in BL depth. When these soundings are reevaluated with the shallow assumption set (75% cloud), a more accurate determination of the depth of the STBL results due to the steeper pseudo-adiabatic lapse rate. Therefore, the process of making a first guess at the depth of the BL transforms the dividing point for the two sets of assumptions into a broader range of depths. For this dataset the effect was to extend the depth from 400m up to 460m in cases where the BL depth was severely underestimated by the assumption of 41% cloud.

3. Sounding Case Studies

Table 3 lists all R/V *Glorita* soundings along with position, launch time and general comments on their analysis. A total of 46 soundings were studied in the sounding application part of this thesis in order to validate the various assumptions made about the properties of the STBL. The following is a breakdown of several soundings that are representative of three primary depth categories. These cases are presented in detail in order to demonstrate how the assumptions described above apply to the various boundary layer depths encountered during this study.

a. GL16

Figure 4-4 shows a plot of sounding GL16 that was launched at 1153 UTC on 11 June 94 at 36.15°N-122.57°W. The surface pressure for this sounding is 1015.0

mb, relative humidity is 98.8%, and winds are from the NNW at 0.3m/s and increasing in strength with height. T_S was not recorded for this case and surface air temperature is 13.2°C. The depth of the boundary layer in this case is 330 meters with a cloud fraction of approximately 75%.

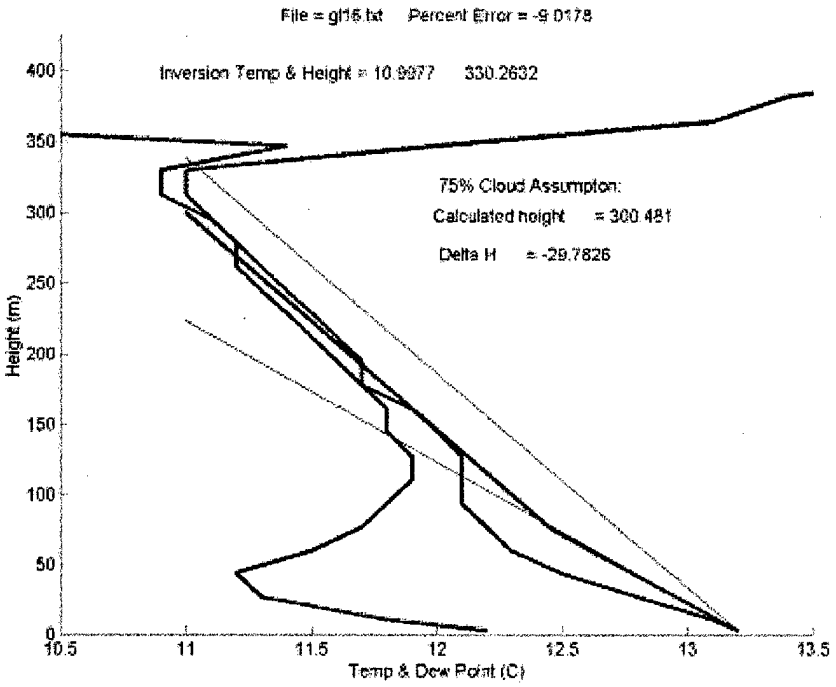

Figure 4-4: Sounding GL16 with lapse rate assumptions of 75% cloud and Γ_m = -6.5°C/km applied.

When the procedure is run on the sounding GL16 the first guess assumption (41% cloud) returns a BL height of 254m which corresponds to a ΔH of –76m or an underestimate of 76m. This falls in the <400m category and the technique requires a shift in the assumption set to the 75% cloud assumption. This combination of lapse rates gives a much more favorable result where the calculated height is now 300m with a ΔH of only –30m.

b. GL67

Figure 4-5 shows a plot of Sounding GL67 that was launched at 1148 UTC on 22 June 94 at 35.78°N-123.18°W. The surface pressure for this sounding is 1019.8 mb, relative humidity is 77.6%, and winds are from the NW at 9.6m/s. Surface air temperature is 14.1°C, but T_S was not recorded for this case. The depth of the boundary layer in this case is 504 meters.

When the procedure is applied to sounding GL67 the first guess assumption of 41% cloud returns a height value that is well above the 400m height and therefore these values will be retained in dealing with this sounding. The 41% cloud assumption returned a calculated height of 507m with a ΔH of +3m.

It is important to note that when this sounding is compared to a satellite image that is described later it can be seen that it passes through an area of reduced cloudiness that is immediately adjacent to a broad area of very even marine stratocumulus clouds. Due to the uniform nature of the surrounding cloudiness it is assumed that the boundary layer properties associated with the surrounding clouds is represented in the sounding GL67 even though the sounding does not pass directly through these clouds.

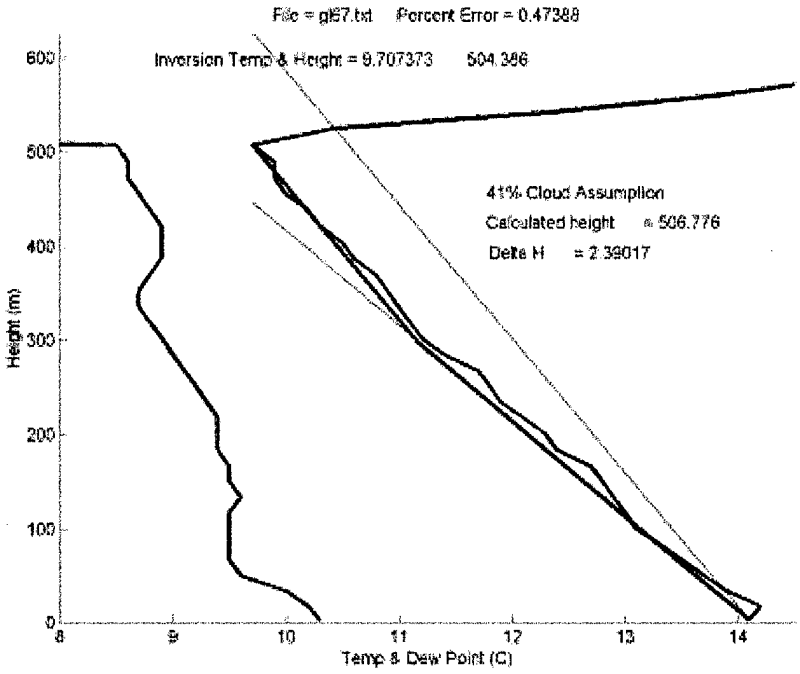

Figure 4-5: Sounding GL67 with lapse rate assumptions of 41% cloud and Γ_m = -7.0°C/km applied.

c. GL68

Figure 4-6 shows a plot of Sounding GL68 that was launched at 1453 UTC on 22 June 94 at 35.70°N-123.46°W. The surface pressure for this sounding is 1021.1 mb, relative humidity is 84.4%, and winds are from the NW at 9.0m/s and decreasing in strength with height. The surface air/sea temperature difference is T_A-T_S = -1.1°C, and the surface air temperature is 14.0°C. The depth of the boundary layer in this case is 671m with a cloud fraction of approximately 37%.

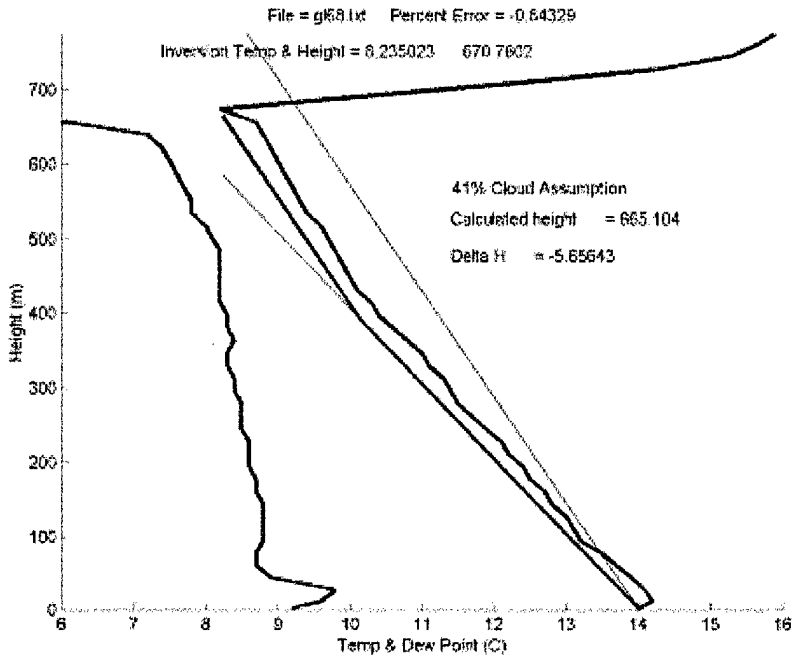

Figure 4-6: Sounding GL68 with lapse rate assumptions of 41% cloud and Γ_m = -7.0°C/km applied.

When the lapse rate procedure is applied to this sounding the first guess assumption is utilized for this case due to the returned boundary layer depth of 665m, which corresponds to a ΔH of –6m. As a test case the actual T_S value (T_S = 15.1°C) was used in this method and the result was an increase in the calculated depth of the boundary layer. This initial temperature modified the result such that an assumption of 41% cloud returns a calculated height of 789m with a ΔH of +118m. This indicates that a 1°C change in surface temperature modifies the height differential value by approximately 120m. The effect of surface and cloud-top temperature variations on the entire sounding dataset will be discussed in section C of this chapter.

d. GL17

Figure 4-7 shows a plot of Sounding GL17 that was launched at 1448 UTC on 11 June 94 at 36.23°N-122.48°W. The surface pressure for this sounding is 1015.5 mb, relative humidity is 99.3%, and winds are from the West at 1.0m/s.

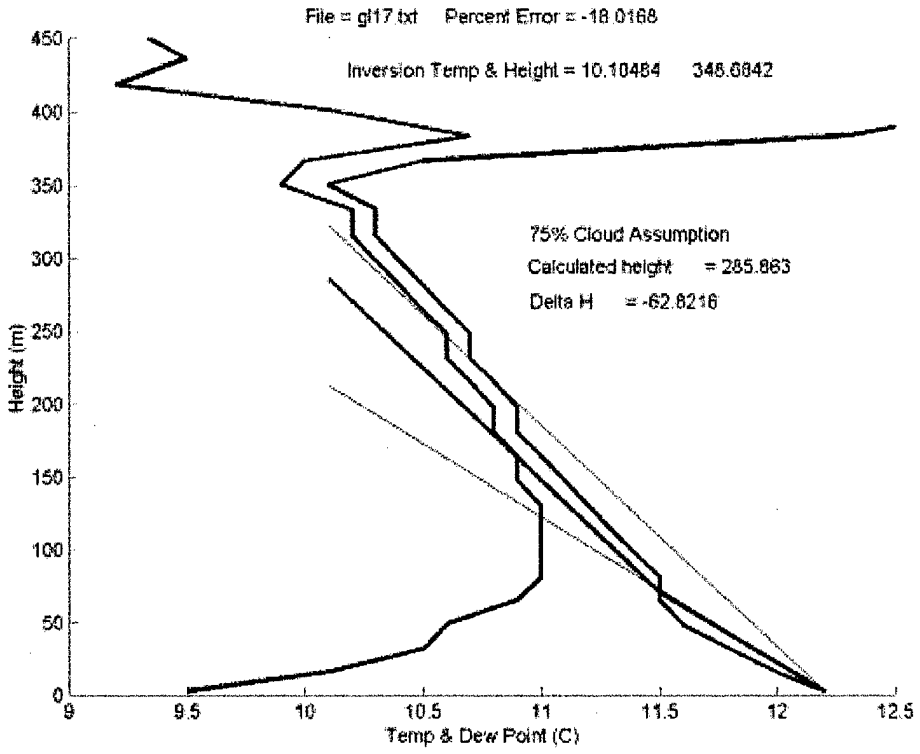

Figure 4-7: Sounding GL17 with lapse rate assumptions of 75% cloud and Γ_m = -6.5°C/km applied.

The surface air temperature for this sounding is 12.2°C and the value of T_S was not recorded for this sounding. The depth of the boundary layer in this case is 340m with a cloud fraction of approximately 88%.

Sounding GL17 is relatively shallow and when the first guess set of assumptions are applied it returns a height of 242m and therefore the 75% cloud

assumption is applied to this sounding. The assumption of 75% cloud gives a calculated BL height of 286m which corresponds to an underestimate of $\Delta H = -54$m.

e. GL29

Figure 4-8 shows a plot of Sounding GL29 that was launched at 2347 UTC on 12 June 94 at 37.05°N-123.25°W. The surface pressure for this sounding is 1016.8 mb, relative humidity is 91.9%, and winds are from the NW at 7.0m/s and increasing in strength with height. The surface air temperature for this sounding is 14.0°C and the air/sea temperature difference is T_A-T_S = -0.6°C. The depth of the boundary layer in this case is 377 meters with a cloud fraction of approximately 23.5%.

This sounding initially meets the conditions necessary to be reevaluated with the assumptions for BLs below 400m. The first guess routine returns a BL depth of 277m with a corresponding height differential of ΔH = -100m. When the assumption of 75% cloud is applied to this sounding is returns a boundary layer height of 327m which corresponds to a height differential of ΔH = -50m.

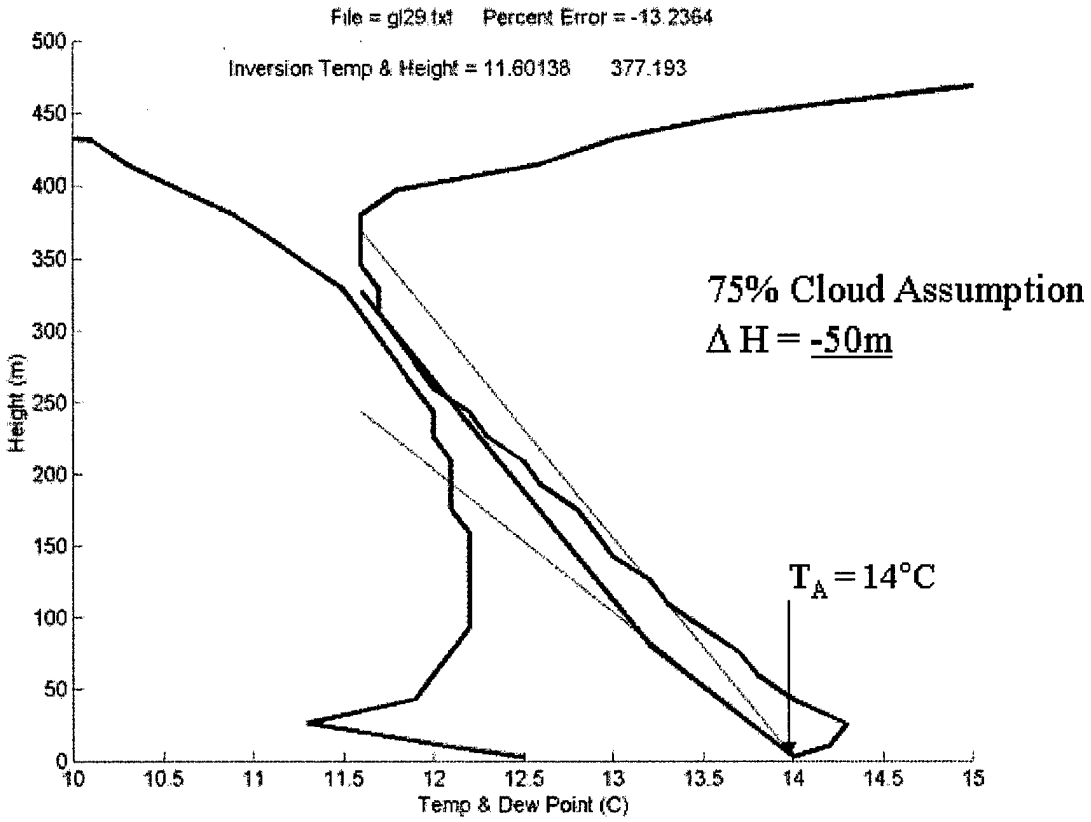

Figure 4-8: Sounding GL29 with lapse rate assumptions of 75% cloud and Γ_m = -6.5°C/km applied.

C. TEMPERATURE VARIATIONS

It was shown in the previous section that variations in surface temperature can have a significant effect on the accuracy of the technique presented in this thesis. Figure 4-9 shows an individual example where sounding GL29 was modified such that the lapse rate is started at the actual sea surface temperature (T_S = 14.6°C).

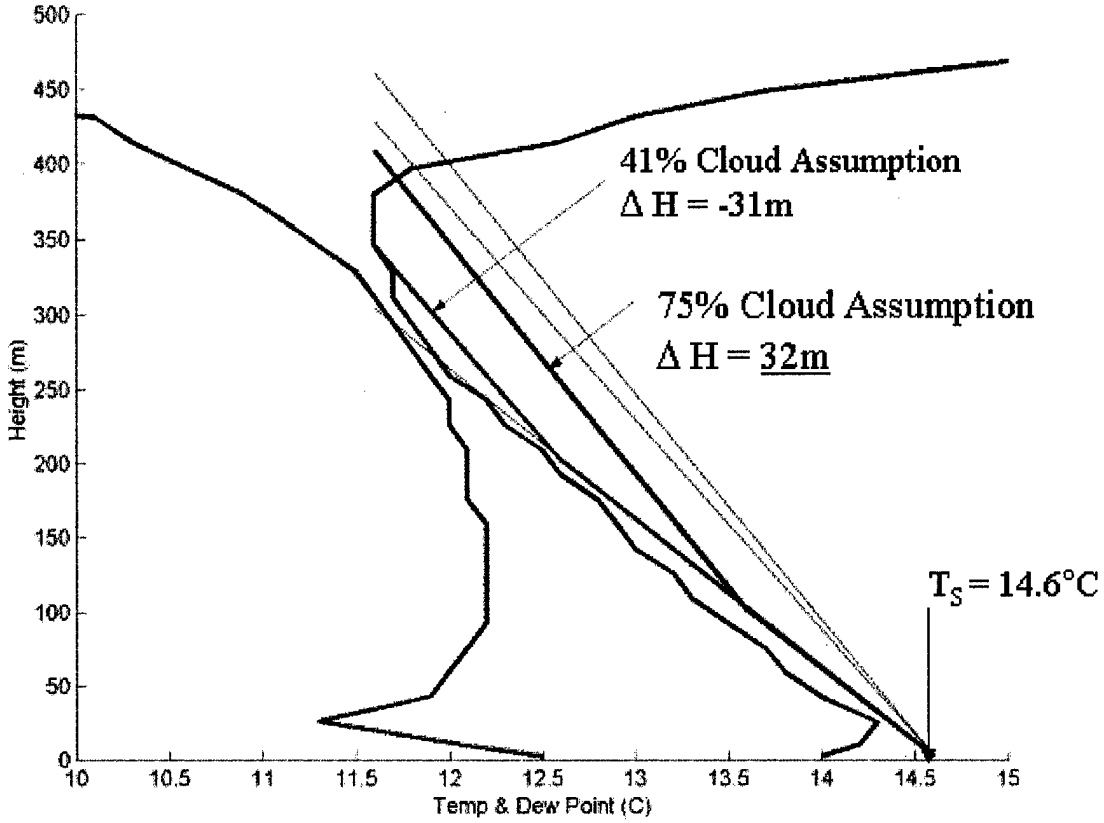

Figure 4-9: Sounding GL29 corrected to start at the actual SST of 14.6°C. The steep, light blue lines represent the two different values for the pseudo-adiabatic lapse rate.

A sensitivity test was made for the entire sounding dataset where both surface and cloud-top temperature were modified. The results of these modifications are compared to the 41% cloud assumption as well as a "no cloud" and an "all cloud" state. Figures 4-10 thru 4-13 demonstrate how an offset in surface and cloud-top temperature (T_S, T_{CT}) affects the accuracy of the model. Figures 4-10 and 4-12 indicate that a ½°C decrease in T_S or a ½°C increase in T_{CT} produces a resulting accuracy that is equivalent to that of a model that relies solely on a dry adiabatic lapse rate for the entire BL. That is, these temperature

changes approximate that of a model that utilizes a dry adiabatic lapse rate over the entire depth of the BL. Figures 4-11 and 4-12 show how a 1°C increase in T_S or a 1°C decrease in T_{CT} produces a result that is equivalent to that of a model that relies solely on a dry adiabatic lapse rate for the entire BL, i.e., a boundary layer completely filled with cloud.

The blue (41% cloud) line as with all of the lines represents a single set of assumptions applied to the entire dataset. The slight increase in error or tail that lies away from and below the main peak represents the shallow cases where Z_{BL} <400m. These figures give a sense of the impact of inaccuracies in both T_S and T_{CT} where even relatively small errors in temperature can have a significant impact on the accuracy of the technique. These results imply that if errors T_{CT} or T_S are greater than 1°C then there is essentially no advantage to breaking up the lapse rates when determining BL depth.

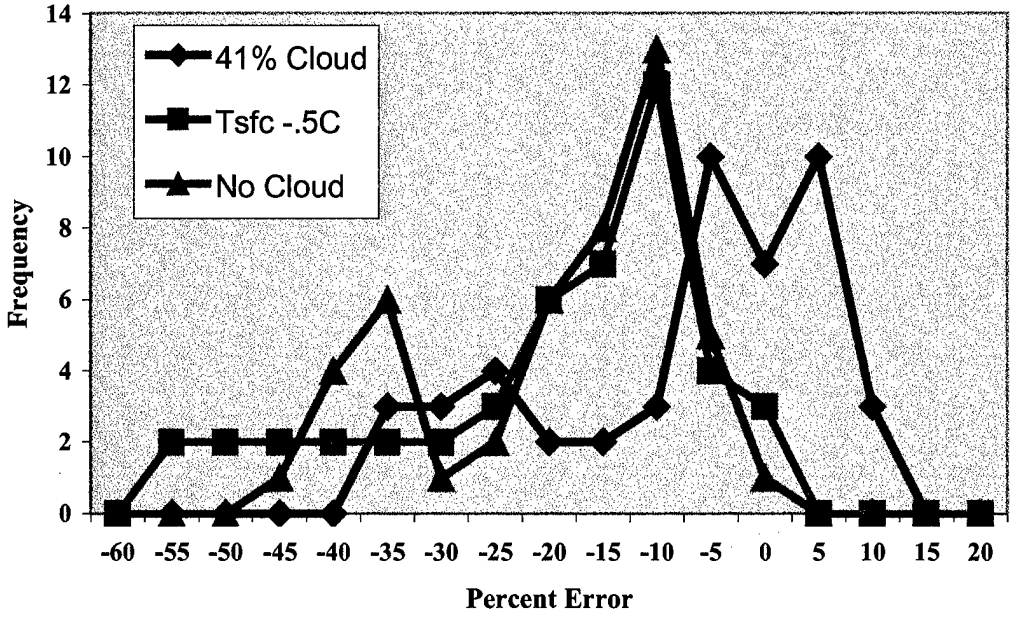

Figure 4-10: The effect of a decrease in surface temperature compared to a cloud-free boundary layer.

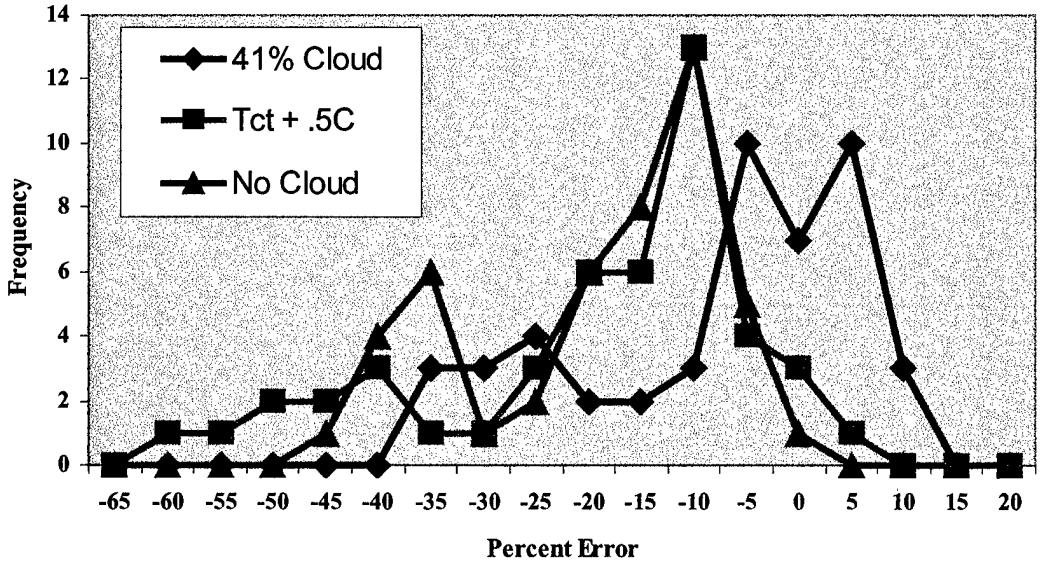

Figure 4-11: The effect of an increase in surface temperature compared to an all-cloud boundary layer.

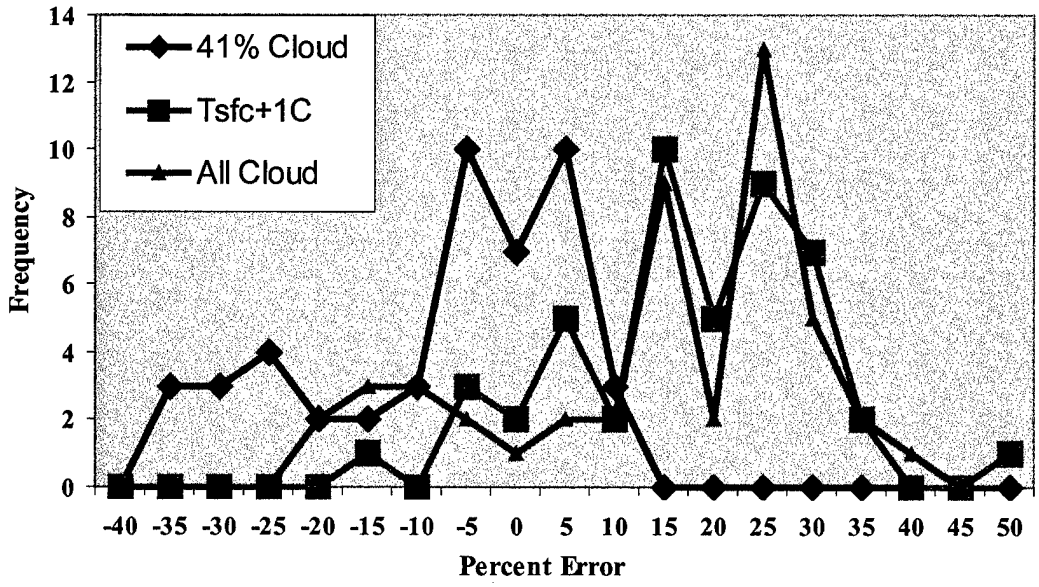

Figure 4-12: The effect of an increase in cloud-top temperature compared to a cloud-free-boundary layer.

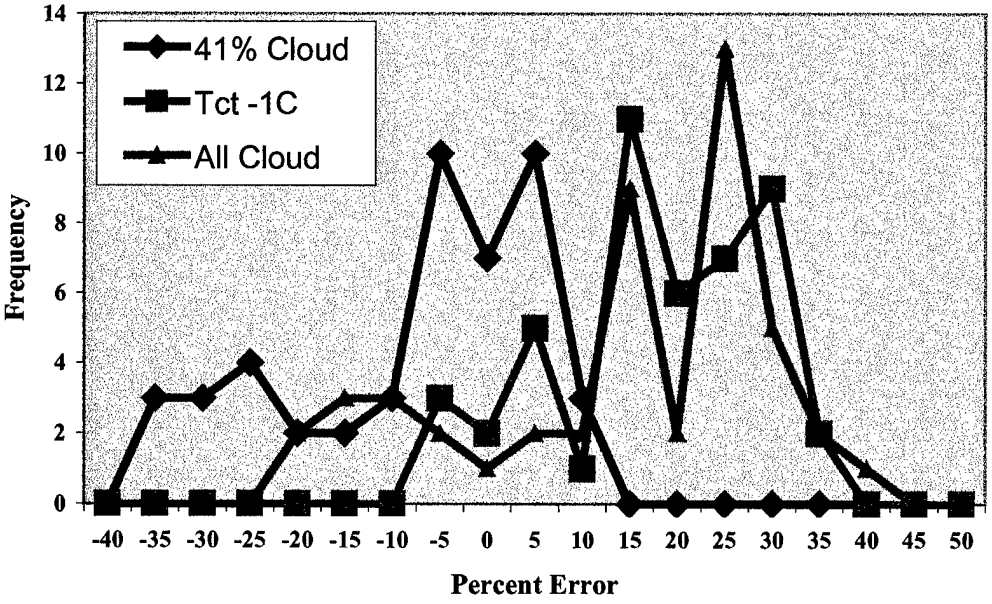

Figure 4-13: The effect of a decrease in cloud-top temperature compared to cloud-free boundary layer.

D. SATELLITE APPLICATION

The sounding profiles from the Glorita were paired with images from NOAA-9,10,11 and 12 that were closest in time to the soundings. Due to the relatively homogeneous nature of environment that produces marine stratocumulus clouds a maximum time difference of three hours was chosen as the criteria to identify sounding/image pairs.

Channel 4 of each satellite image was analyzed in the region that the sounding was taken in order to determine the cloud top temperature. However, the presence of cirrus clouds in the image caused some cases to be dismissed. Cirrus clouds, being much colder than MABL clouds, contaminated the brightness temperature and produce erroneous results that significantly overestimate the depth of the STBL. Therefore, this method is not valid for images with significant cirrus contamination. For detailed information on which soundings were utilized for this procedure and which were dismissed see Table 4 in Appendix A.

The technique applied to the sounding dataset was applied to satellite imagery in order to evaluate the accuracy of the application of T_B measurements that are utilized as cloud-top temperature. The value of T_S in this part of the study was once again obtained from the sounding in order to better understand the accuracy of substituting T_B for T_{CT}. The returned values of BL height were plotted against the actual BL height with the actual BL height as the independent variable.

Figures 4-14 and 4-15 show a linear regression was performed on the data points in order to determine the accuracy of the process for both the direct method and the first

guess method respectively. The result from the first guess method was again found to be even more accurate than the direct (single assumption set) application. A linear regression of the direct method returned a slope of 1.3074, an offset of –153m and an overall error estimate of 76m. The regression of the first guess method returned a line with a slope of 1.2687, an offset of –137m and an overall error of 65m. The details of this application and how it compared to the ground truth of the soundings can be seen Table 2 in Appendix A.

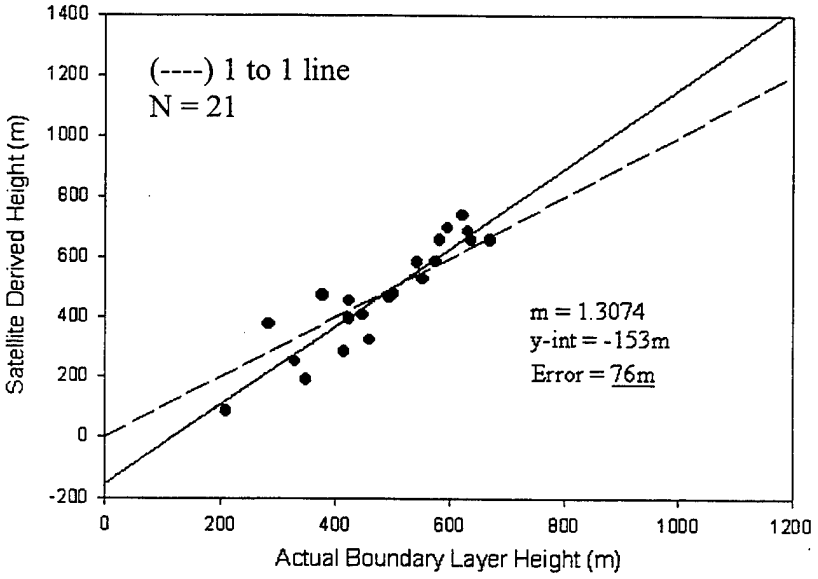

Figure 4-14: Linear regression of actual vs. calculated boundary layer height using satellite derived T_B data. The solid line is the regression line.

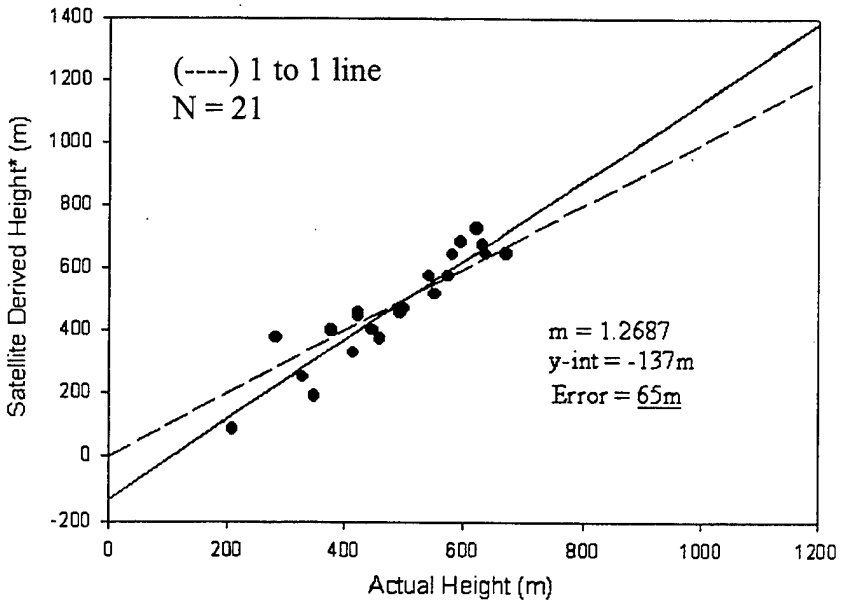

Figure 4-15: Linear regression of actual vs. calculated boundary layer height using satellite T_B data. The solid line is the regression line.
*- Heights obtained using "first guess" process.

1. Favorable Satellite Case Studies

The accuracy of using satellite T_B as cloud-top temperature in the technique described above will be illustrated below for three sounding image pairs.

a. GL16

Figure 4-16 shows the closest satellite image associated with sounding GL16 that was taken at 2349 UTC on 27 June 94. The visual image in the area of this sounding shows a uniform sheet of stratocumulus cloud.

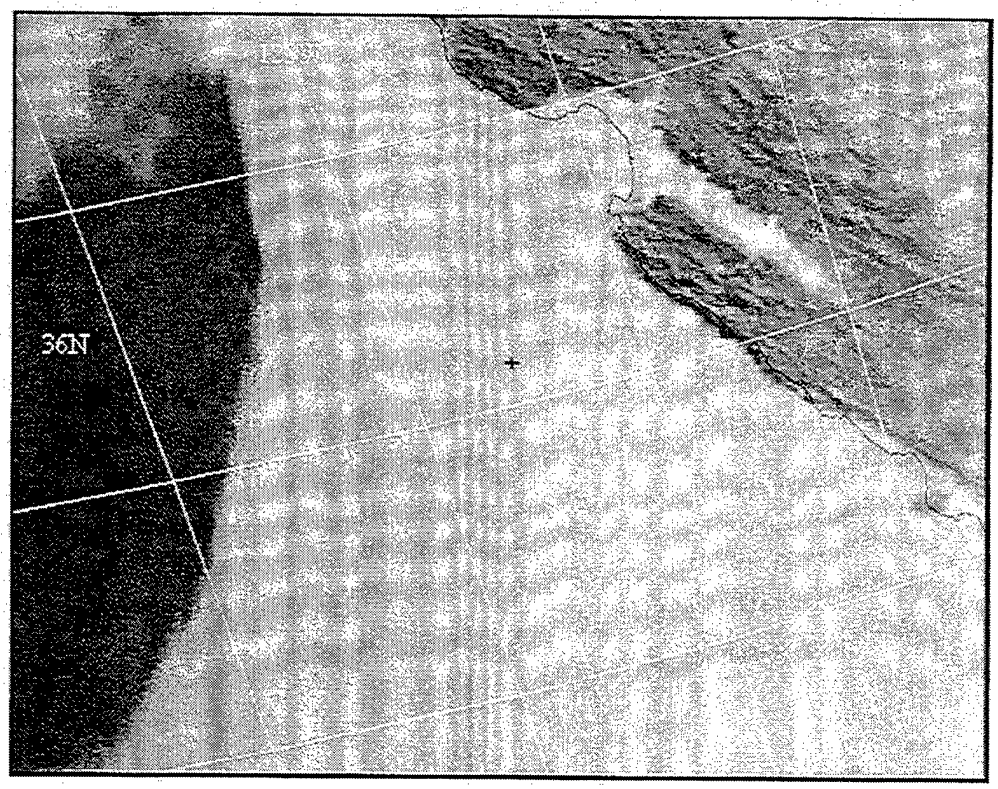

Figure 4-16: AVHRR Channel 2 image for GL16.

Figure 4-17 shows the corresponding T_B taken from the IR image has a value of 11.4°C, which is very close in magnitude to the sounding cloud-top temperature (11.0°C). The application of this T_B to the lapse rate calculation of BL height yields a height of 251m (ΔH = -79m).

Figure 4-17: AVHRR channel 4 image for GL16.

For comparison the sounding based technique had a height differential of ΔH = -30m showing that, for this situation, a 49m change in accuracy resulted from a T_{CT} error of +0.4°C.

b. GL67

Figure 4-18 shows the image that most closely corresponds to sounding GL67 was taken at 1148 UTC on 22Jun94. The corresponding T_B taken from the IR image has a value of 10.0°C, which is very close in magnitude to the sounding cloud-top temperature (9.7°C).

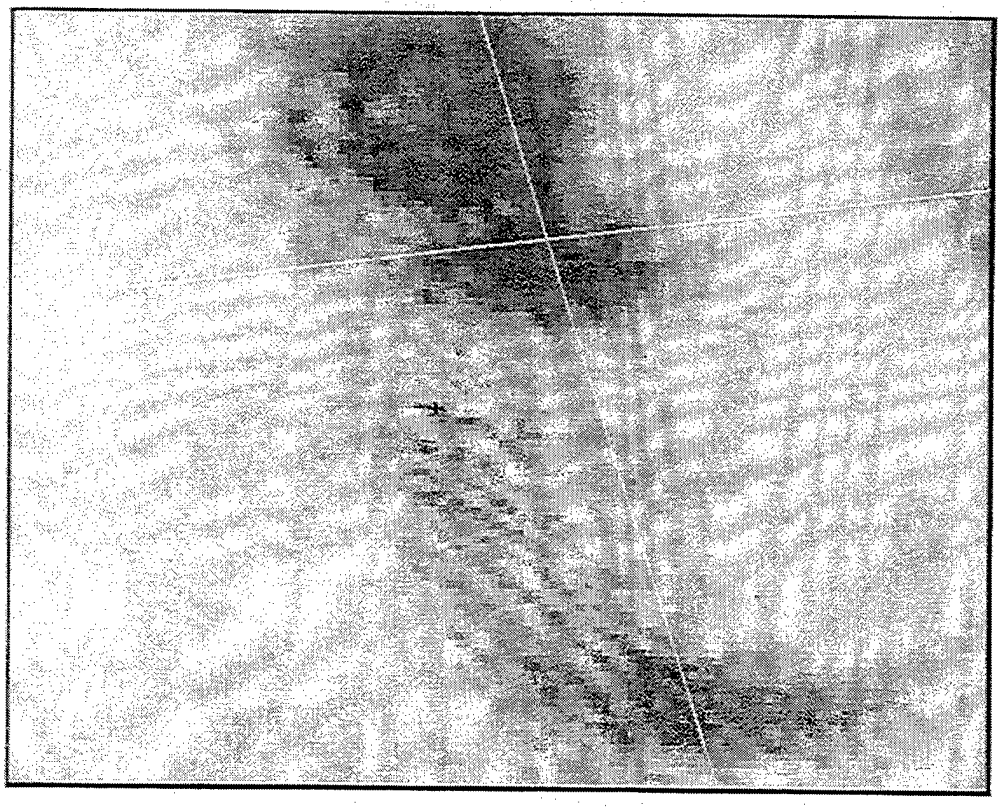

Figure 4-18: AVHRR Channel 4 zoomed image from for GL67

The sounding in this case appears to go through a region of thin cloud the details of which can be clearly seen in Figure 4-18. The corresponding value of T_B measured in the IR image was obtained from the nearby thicker cloud which were assumed to be representative of the BL in the vicinity of sounding GL67. The application of this T_B to the lapse rate calculation of BL height yields a height of 477m (ΔH = -29m). For comparison the sounding based technique had a height differential of ΔH = +3m showing that, for sounding GL67, a 32m change in accuracy resulted from a T_{CT} error of +0.3°C.

c. GL68

The image that most closely corresponds to sounding GL68 was taken at 1514 UTC on 22Jun94. The visual image (Figure 4-19) in the area of this sounding shows a region of even, well distributed stratocumulus clouds.

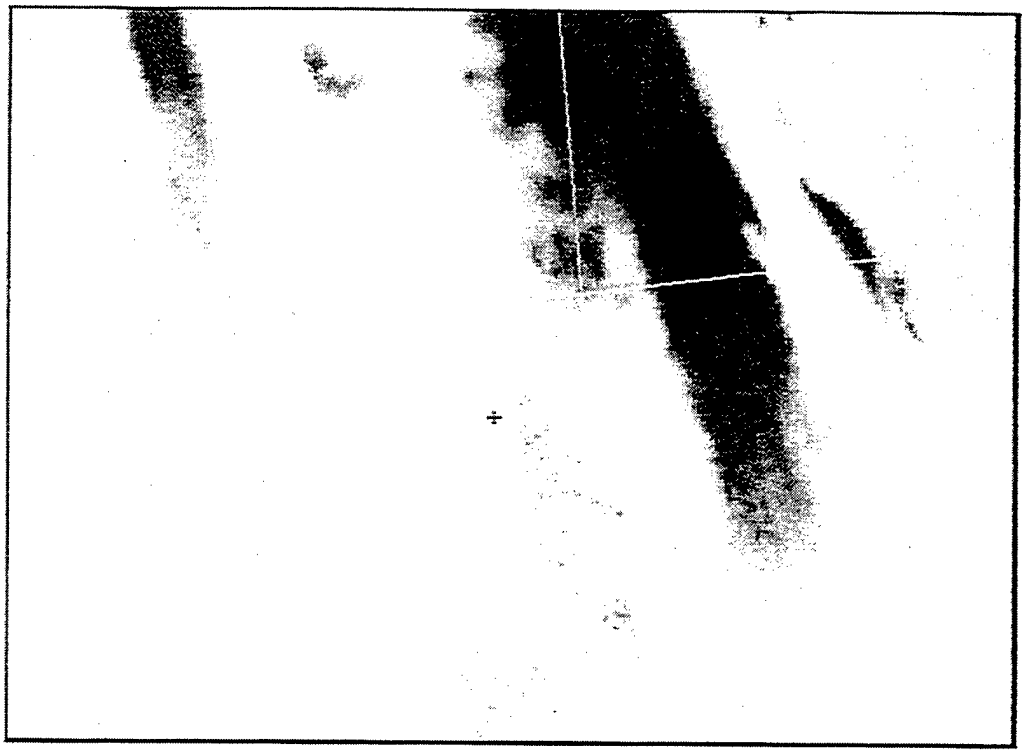

Figure 4-19: AVHRR channel 2 image for GL68.

The corresponding T_B taken from the IR image (Figure 4-20) has a value of 8.4°C, which is very close in magnitude to the sounding cloud-top temperature (8.2°C). The application of this T_B to the lapse rate calculation of BL height yields a height of 647m (ΔH = -24m). For comparison the sounding based technique had a height differential of ΔH = -6m showing that, for this situation, a 18m change in accuracy resulted from a T_{CT} error of +0.2°C.

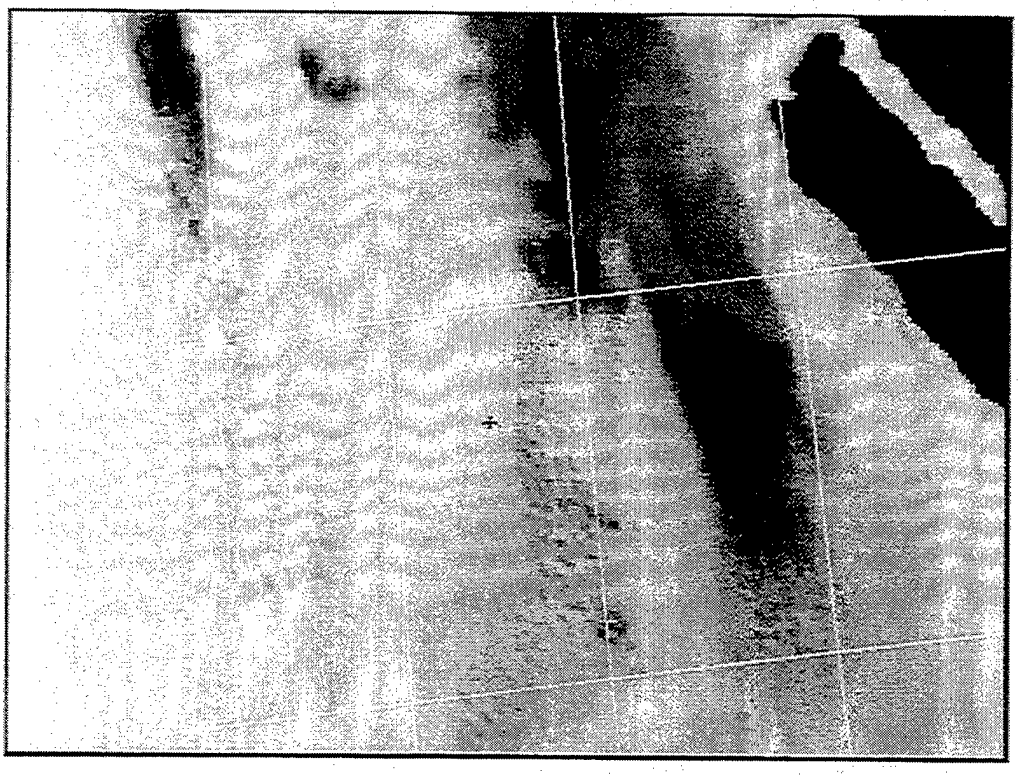

Figure 4-20: AVHRR channel 4 image for GL68.

2. Unfavorable Satellite Case Studies

There are several situations where the accurate retrieval of T_{CT} from satellite imagery is not possible. Errors in T_{CT} can occur when there are higher clouds (e.g., cirrus) above the STBL, or when there is a shallow BL where the clouds are too thin and permit radiance from the surface to contaminate the T_B readings. The latter case will be illustrated below as will an instance of "limb darkening" where T_B are obtained from the far edges of the satellite path.

a. GL17

The closest satellite image associated with sounding GL17 was taken at 1551 UTC on 11 June 94. This image can be seen on Figures 4-21 and 4-22, which show the visual (channel 2) and the infrared (channel 4) respectively.

Figure 4-21: AVHRR channel 2 image for GL17.

The brightness temperature derived from channel 4 for this image was 10.8°C, which is slightly warmer than the cloud-top temperature measured on the sounding (10.1°C). This increase in T_B is possible due to the influence of continental aerosols that reduce droplet size and absorptance in the stratocumulus clouds leading to radiance from lower in the cloud contributing to T_B and producing higher values of T_B (Brenner, J.R., 1994).

The sounding technique results that were described previously in this chapter returned a BL height of 286m or an underestimate of $\Delta H = -64m$. The application of the warmer T_B from the satellite image produced an enhancement of this underestimate and returned a BL height of 192m or a $\Delta H = -157m$. This indicates that there was a 93m change in accuracy due to a +0.7°C change in T_{CT}.

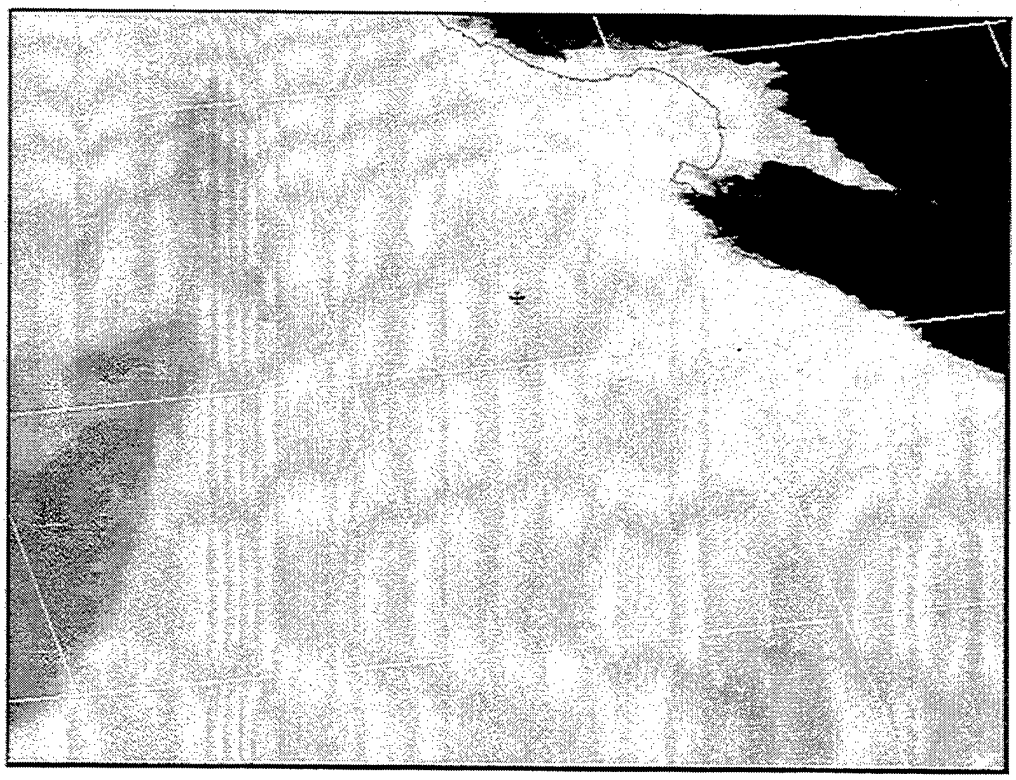

Figure 4-22: AVHRR channel 4 image for GL17.

b. GL82

Sounding GL82 was launched at 2349 UTC on 27 June 94 at 35.17°N-124.82°W. The surface pressure for this sounding is 1021.8mb, relative humidity is 83.8%, and winds are from the NNW at 9.2m/s. The surface air/sea temperature

difference is T_A-T_S = 0.0°C, and the surface air temperature is 16.1°C. The depth of the boundary layer in this case is 640m with a cloud fraction of approximately 34.3%.

The closest satellite image associated with sounding GL82 was taken at 2334 UTC on 27 June 94. Figure 4-23 shows the IR satellite image for GL82. The image shows that the corresponding sounding position was on the far left-hand side of the swath. This situation falls into the "limb darkening" category where radiance from the position of the sounding is reduced in intensity due to the extreme angle at which it travels to reach the satellite sensor.

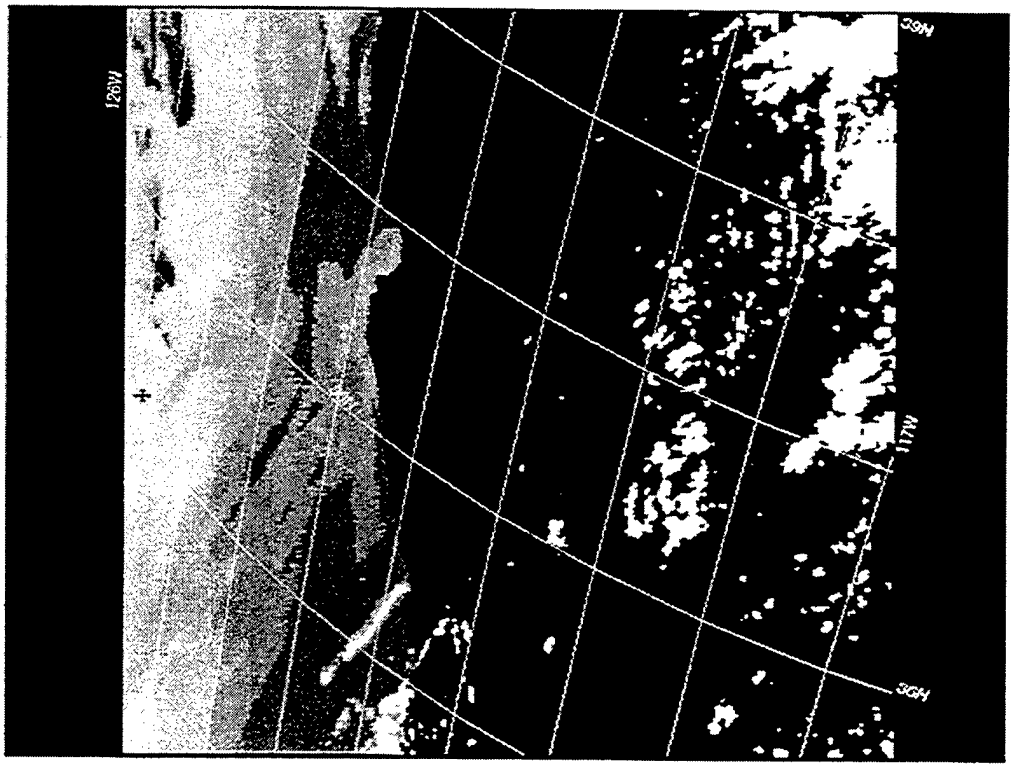

Figure 4-23: AVHRR channel 4 image for GL82.

The channel 4 brightness temperature measured at the location of the sounding on Figure 4-23 has a value of 9.1°C, which is significantly colder than the

corresponding cloud-top temperature taken from sounding GL82 (T_{CT} = 10.2°C). This temperature differential results in a calculated BL depth of 808m which corresponds to a height differential of $\Delta H = +168m$.

3. Large Scale Satellite Application

The next step in the logical progression of this technique is to apply it to the entire image vice a single point. This was done using a single T_S measurement from sounding GL62 to represent the entire T_S field along with the corresponding AVHRR image shown in Figures 2-24 and 4-25 that were taken at 1535 UTC on 21 June 94. The result of this process can be seen in Figure 4-26 which represents a topographic map of BL depth off the coast of California. The image shows the depth of the boundary layer increasing away from the coast, which agrees with existing theories on boundary layer depth near coastlines (Stull, R.B., 1988). Depth (in meters) can be determined on the image by use of the color scale located on the upper left-hand side of the image. The image contained higher clouds (seen in the contrast between Figures 24 and 25) and cloud free areas which were filtered out and appear black on the image.

Figure 4-24: AVHRR channel 2 image for sounding GL62.

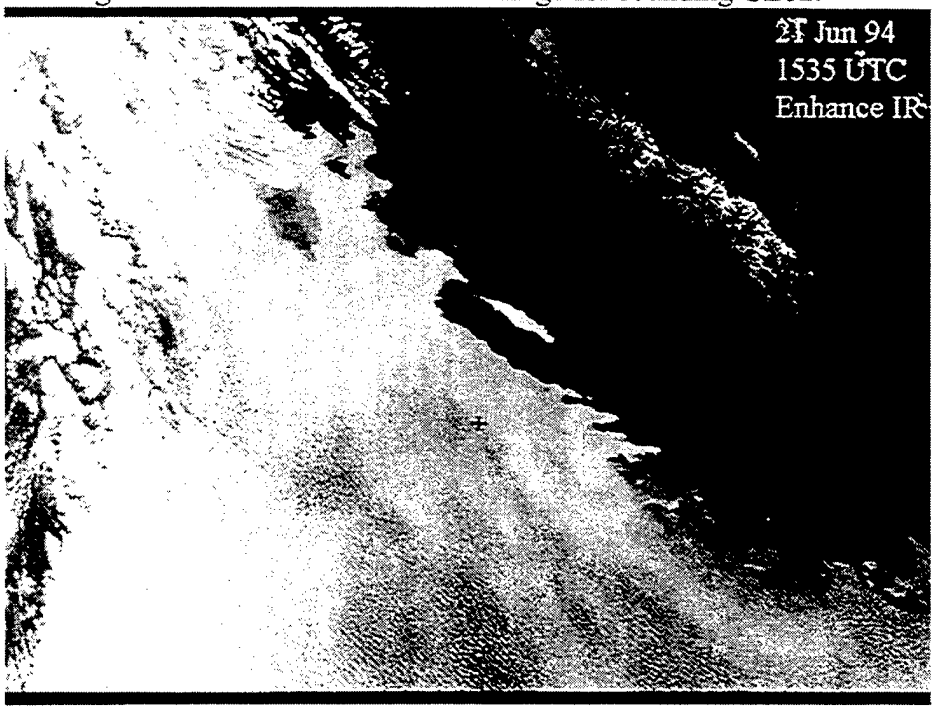

Figure 4-25: AVHRR channel 4 Enhanced IR image of GL62.

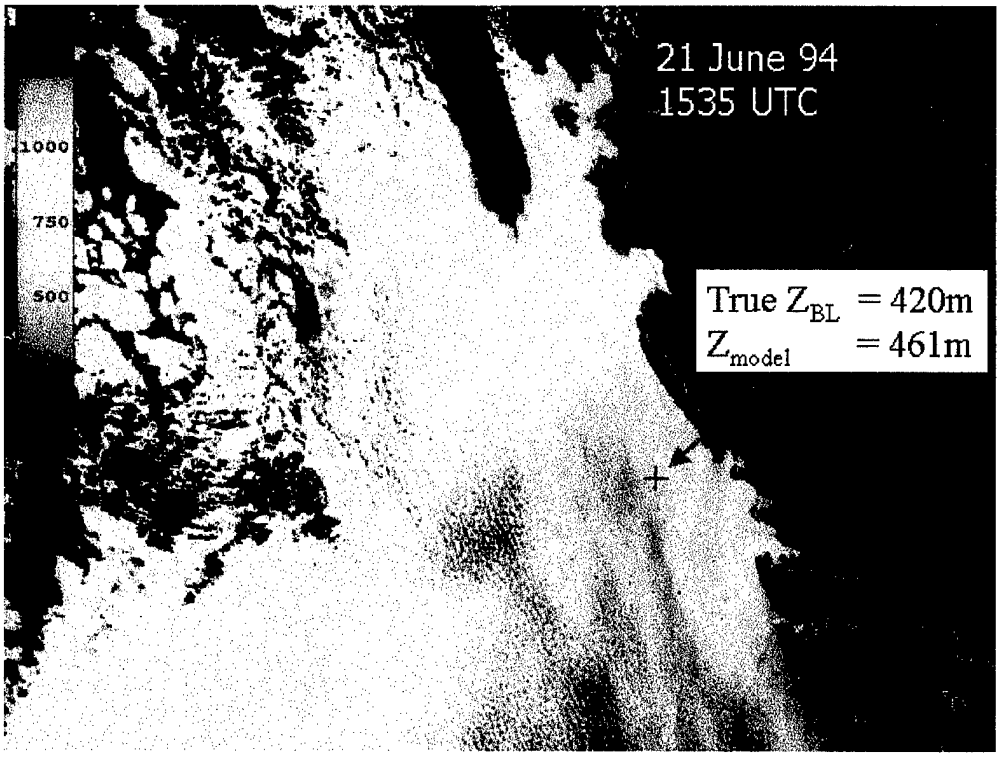

Figure 4-26: Topographic map of BL depth based on sounding GL62's SST, and AVHRR channel 4 imagery. The red cross indicates the location of sounding GL62.

THIS PAGE INTENTIONALLY LEFT BLANK

V. CONCLUSIONS AND RECOMMENDATIONS

A. CONCLUSIONS

The purpose of this thesis was to develop and test a technique for determining the depth of the STBL using boundary layer thermodynamics. The technique determines BL depth by utilizing satellite derived cloud-top brightness temperature and sea surface temperature observations. The method was initially refined with sounding data from the MAST experiment which were used to verify the technique. The technique was then applied to satellite brightness temperature data in place of the cloud-top temperature from the soundings.

Analysis of the MAST dataset revealed that an assumption of 41% cloud (59% cloud-free) with a moist lapse rate of $\Gamma_m = -7.0°C/km$ produced the best overall fit to the data. However, for shallow boundary layers the most accurate assumption set was 75% cloud with a lapse rate of $\Gamma_m = -6.5°C/km$. The shallow cases were found to apply to boundary layers with depths less than 400m. The value of 400m was chosen because it was found to be the center of a gradual shift in the accuracy of the two assumption sets.

The sensitivity of the technique was analyzed by varying the values of both surface, and cloud-top temperatures. Analysis revealed that a ½°C change in either temperature resulted in an error in calculated BL depth of 60-70m. The magnitude of BL height error was found to vary linearly due to the linearity of the lapse rates used in the calculation of BL depth. The sensitivity of this technique to temperature inputs implies a strong need for accurate T_S and T_{CT} fields whenever this technique is used.

This technique is applicable to regions where the atmosphere above the BL is essentially cloud free as cirrus clouds significantly impair the accurate determination of T_B from the STBL. Furthermore, the technique presented here was designed for coupled BLs in a uniform cloud field. This technique will not yield accurate results if applied to decoupled BLs.

B. RECOMMENDATIONS

This study quantitatively demonstrates the sensitivity of BL depth determination to the accuracy of surface and cloud-top temperature data. Models that generate surface temperature data are generally of much lower resolution than the 1km accuracy of AVHRR T_B data. Future work in this area should ensure that the resolution of both T_S and T_{CT} fields are compatible. The application of T_S data to the procedure presented in this study will introduce errors due to differences between T_S and surface air temperature. The errors introduced into the technique due to this difference could be minimized if surface air temperature was obtained from a coupled model that could account for air/sea temperature differences.

Another area of refinement is in the sensitivity of remotely sensed cloud-top temperature to cloud thickness. Measurements of T_B taken from thin clouds can be contaminated with surface radiance, which makes the value of T_B too high. Multi-channel remote sensing techniques can be employed to estimate cloud optical thickness and correct the measured T_B to account for contamination from radiance below the cloud-top.

The application of this technique to EM propagation and ducting conditions can be refined with the application of multi-spectral remote sensing techniques. Multi-spectral techniques could be employed to enhance the determination of the moisture content above the boundary layer which will help with the determination of refractivity conditions (i.e., ducting).

Additional study should be done with this technique in order to better determine the nature of shallow BLs (<400m) and BLs deeper than 700m. Boundary layers shallower and deeper than 400m and 700m respectively were not well represented in this study. The technique presented in this study was not sufficiently sophisticated to deal with complexity inherent in decoupled boundary layers. Therefore, another area for further research is the development of a technique to account for decoupling processes within the STBL.

The ability to estimate boundary layer depth from satellite data is a valuable additional tool for mapping the coastal battlespace or operations areas. In addition, boundary layer depth analyses could provide valuable additional data for local mesoscale models that have been deployed recently. This study points to the way for an important new qualitative use of satellite data to support Navy operations.

THIS PAGE INTENTIONALLY LEFT BLANK

APPENDIX A. TABLES

This appendix serves as a convenient location in order to consolidate the tables discussed in the text of this thesis.

Table 1: Cloud amount and lapse rate assumptions and how they affect the accuracy when compared to the actual height of the STBL.

Cloud Amount (fraction of BL)	Lapse Rate (°C/Km)	Linear Regression Slope	Y-intercept offset (m)	Overall Error Estimate (m)
75% Cloud <400m) 41% Cloud >400m)	-6.5 <400m -7.0 >400m	1.0283	-41	56
75% Cloud <400m* 41% Cloud >400m*	**-6.5 <400m* -7.0 >400m***	**1.0080**	**-24**	**50**
75% Cloud	-7.0	1.2174	-93	60
75% Cloud	-6.5	1.2949	-103	64
60% Cloud	-7.0	1.1488	-86	58
60% Cloud	-6.5	1.2117	-98	61
41% Cloud	-7.0	1.0861	-82	53
41% Cloud	-6.5	1.1236	-85	54

*- Denotes "first guess" process to determine the 400m dividing line for the two sets of assumptions.

Table 2: A comparison of how the accuracy of the technique was affected by using T_B for the T_{CT} vice sounding based T_{CT}.

	Cloud Amount (fraction of boundary layer)	Lapse Rate (°C/Km)	Linear Regression Slope	Y-intercept offset (m)	Overall Error Estimate (m)
Sounding Based Results** - All Soundings	75%Cloud (<400m) 41% Cloud (>400m)	-6.5 (<400m) -7.0 (>400m)	1.0080	-24	50
Sounding Based Results** - Satellite Equivalent Sample	Same as above	Same as above	0.9975	-23	49
Satellite T_B Results*	Same as above	Same as above	1.3074	-153	76
Primary Satellite T_B Results**	Same as above	Same as above	1.2687	-137	65

The "satellite equivalent sample" indicates that the same soundings used for the satellite-based results were extracted from the full sounding set and run separately.

* - Indicates the assumptions were divided according to the previously known (actual) height of the BL.

** - Denotes "first guess" process to determine the 400m dividing line for the two sets of assumptions.

Table 3: MAST experiment soundings, with their corresponding position, time and analysis.

Sounding Number	Latitude, Longitude	Launch Time (date – UTC)	Analysis
GL01	34.15°N 119.21°W	03Jun - 0029	Dismissed – test sounding
GL02	34.16°N 119.27°W	05Jun - 2357	Dismissed – no cloud
GL03	35.25°N 121.16°W	06Jun - 1447	Dismissed – no cloud
GL04	35.98°N 121.65°W	- 2039	Dismissed – no cloud
GL05	36.63°N 122.00°W	08Jun - 0535	Dismissed – no cloud
GL06	35.73°N 122.22°W	- 1149	Dismissed – no cloud
GL07	35.16°N 122.44°W	- 1737	Dismissed – no cloud
GL08	35.29°N 122.46°W	- 2353	Dismissed – no cloud
GL09	36.61°N 121.89°W	10Jun – 1739	Dismissed – no cloud
GL10	36.45°N 122.07°W	- 1929	Dismissed – no cloud
GL11	36.27°N 122.18°W	- 2058	Dismissed – no cloud
GL12	36.08°N 122.18°W	- 2354	Conducive
GL13	36.25°N 122.48°W	11Jun - 0252	Dismissed - too shallow
GL14	36.26°N 122.99°W	- 0549	Conducive
GL15	36.26°N 123.00°W	- 0838	Dismissed – bad sounding
GL16	36.15°N 122.57°W	- 1153	Conducive
GL17	36.23°N 122.48°W	- 1448	Conducive
GL18	36.52°N 122.30°W	- 1746	Conducive

Table 3 continued.

GL19	36.35°N 122.31°W	- 2041	Conducive
GL20	36.66°N 122.41°W	- 2343	Conducive
GL21	36.86°N 122.67°W	12Jun - 0244	Dismissed – no cloud
GL22	37.07°N 122.97°W	- 0541	Dismissed – no cloud
GL23	37.3°N 123.26°W	- 1146	Dismissed – bad sounding
GL24	37.23°N 123.22°W	- 1448	Dismissed – bad sounding
GL25	36.99°N 122.89°W	- 1732	Conducive
GL26	36.90°N 123.06°W	- 2020	Conducive
GL27	36.96°N 123.14°W	- 2132	Conducive
GL28	37.05°N 123.25°W	- 2347	Conducive
GL29	37.19°N 123.40°W	13Jun - 0242	Conducive
GL30	36.95°N 123.01°W	- 0549	Conducive
GL31	36.65°N 122.77°W	- 0841	Conducive
GL32	36.31°N 122.69°W	- 1143	Conducive
GL33	36.01°N 122.60°W	- 1451	Conducive
GL34	36.07°N 122.56°W	- 1741	Dismissed – bad sounding
GL35	36.05°N 122.75°W	- 2030	Dismissed – no cloud
GL36	36.33°N 123.16°W	- 2338	Dismissed – no cloud
GL37	36.35°N 122.65°W	14Jun - 0242	Dismissed – no cloud
GL38	36.53°N 122.16°W	- 0537	Dismissed – no cloud

Table 3 continued.

GL39	36.14°N 122.08°W	15Jun - 1740	Dismissed – no cloud
GL40	35.46°N 122.26°W	-2324	Dismissed – no cloud
GL41	35.50°N 122.42°W	16Jun - 0257	Dismissed – no cloud
GL42	35.69°N 122.61°W	- 0542	Dismissed – no cloud
GL43	35.20°N 123.25°W	- 1145	Conducive
GL44	35.32°N 123.64°W	- 1456	Dismissed – no cloud
GL45	35.50°N 123.78°W	- 1735	Dismissed – no cloud
GL46	35.61°N 123.90°W	- 2030	Dismissed – no cloud
GL47	35.85°N 124.00°W	- 2335	Dismissed – no cloud
GL48	36.09°N 124.12°W	17Jun - 0244	Dismissed – no cloud
GL49	36.30°N 124.23°W	- 0545	Dismissed – no cloud
GL50	36.51°N 122.33°W	- 0841	Dismissed – no cloud
GL51	36.73°N 124.41°W	- 1156	Conducive
GL52	36.85°N 124.29°W	- 1448	Conducive
GL53	36.85°N 123.76°W	- 1804	Dismissed – no cloud
GL54	36.76°N 122.73°W	- 2348	Dismissed – no cloud
GL55	36.72°N 122.01°W	20Jun - 1458	Conducive
GL56	36.77°N 122.42°W	- 1809	Conducive
GL57	36.56°N 122.59°W	- 2358	Dismissed – no cloud

Table 3 continued.

GL58	36.24°N 122.54°W	21Jun - 0233	Dismissed – no cloud
GL59	35.88°N 122.37°W	- 0551	Dismissed – no cloud
GL60	35.54°N 122.13°W	-0847	Conducive
GL61	35.15°N 121.90°W	- 1150	Conducive
GL62	35.11°N 121.85°W	- 1503	Conducive
GL63	35.11°N 121.88°W	- 1751	Conducive
GL64	34.83°N 121.77°W	- 2053	Conducive
GL65	35.02°N 122.06°W	- 2352	Dismissed – no cloud
GL66	35.22°N 122.27°W	22Jun – 0244	Dismissed – no cloud
GL67	35.78°N 123.18°W	- 1148	Conducive
GL68	35.70°N 123.46°W	- 1453	Conducive
GL69	35.26°N 123.58°W	- 1752	Conducive
GL70	34.98°N 123.73°W	- 2046	Dismissed – no cloud
GL71	35.27°N 123.65°W	- 2346	Dismissed – no cloud
GL72	35.58°N 123.32°W	23Jun – 0249	Dismissed – no cloud
GL73	35.88°N 123.02°W	- 0545	Dismissed – no cloud
GL74	35.50°N 122.06°W	- 2006	Dismissed – no cloud
GL75	36.65°N 121.94°W	26Jun – 0546	Dismissed – no cloud
GL76	35.90°N 123.01°W	- 1453	Dismissed – no cloud

Table 3 continued.

GL77	35.10°N 123.67°W	- 2151	Dismissed – no cloud
GL78	34.53°N 124.02°W	27Jun – 0241	Conducive
GL79	34.40°N 124.78°W	-1452	Conducive
GL80	34.54°N 124.84°W	-1801	Conducive
GL81	34.78°N 124.83°W	- 2053	Conducive
GL82	35.17°N 124.84°W	- 2349	Conducive
GL83	35.44°N 124.82°W	28Jun – 0238	Conducive
GL84	35.71°N 124.66°W	- 0545	Conducive
GL85	35.33°N 124.52°W	- 0855	Conducive
GL86	35.03°N 124.03°W	- 1150	Conducive
GL87	35.11°N 123.89°W	- 1451	Conducive
GL88	35.33°N 124.07°W	- 1800	Conducive
GL89	35.55°N 124.25°W	- 2057	Conducive
GL90	35.74°N 124.44°W	-2344	Conducive
GL91	35.91°N 124.58°W	29Jun – 0249	Conducive
GL92	35.58°N 124.37°W	- 0547	Conducive
GL93	35.38°N 124.00°W	- 0841	Conducive
GL94	34.94°N 122.71°W	- 1645	Conducive

Table 4: MAST experiment soundings, corresponding satellite images and analysis.

Sounding Number	Launch Time (date – UTC)	Corresponding Satellite Image (date; sat; UTC)	Analysis
GL12	10Jun - 2354	11Jun; n11; 0119	Conducive
GL14	11Jun - 0549	n9; 0530	Conducive
GL16	- 1153	n11; 1342	Conducive
GL17	- 1448	n12; 1551	Conducive
GL18	- 1746	n9; 1753	Conducive
GL19	- 2041	none	Dismissed – no image
GL20	- 2343	n11; 2327	Conducive
GL25	12Jun - 1732	12Jun; n9; 1740	Dismissed – cirrus contamination
GL26	- 2020	none	Dismissed – no image
GL27	- 2132	none	Dismissed – no image
GL28	- 2347	13Jun; n11; 0057	Dismissed – cirrus contamination
GL29	13Jun - 0242	n12; 0249	Dismissed – cirrus contamination
GL30	- 0549	n9; 0503	Dismissed – cirrus contamination
GL31	- 0841	none	Dismissed – no image
GL32	- 1143	n11; 1318	Dismissed – cirrus contamination
GL33	- 1451	n12; 1508	Dismissed – cirrus contamination
GL43	16Jun - 1145	16Jun; n11; 1241	Dismissed – cirrus contamination
GL51	17Jun - 1156	17Jun; n11; 1229	Dismissed – cirrus contamination
GL52	- 1448	n11; 1410	Dismissed – cirrus contamination

Table 4 continued.

GL55	20Jun - 1458	20Jun; n10; 1455	Dismissed – cirrus contamination
GL56	- 1809	n9; 1737	Conducive
GL60	21Jun - 0847	none	Dismissed – no image
GL61	- 1150	21Jun; n11; 1320	Conducive
GL62	- 1503	N12; 1535	Conducive
GL63	- 1751	N9; 1724	Conducive
GL64	- 2053	None	Dismissed – no image
GL67	22Jun - 1148	22Jun; n11; 1308	Conducive
GL68	- 1453	n12; 1514	Conducive
GL69	- 1752	n9; 1711	Conducive
GL78	27Jun – 0241	27Jun; n12; 0246	Dismissed – cirrus contamination
GL79	- 1452	n12; 1506	Dismissed – limb darkened
GL80	- 1801	n9; 1747	Conducive
GL81	- 2053	none	Dismissed – no image
GL82	- 2349	n11; 2332	Dismissed – limb darkened
GL83	28Jun – 0238	28Jun; n12; 0246	Conducive
GL84	- 0545	n9; 0511	Conducive
GL85	- 0855	none	Dismissed – no image
GL86	- 1150	none	Dismissed – no image
GL87	- 1451	n10; 1503	Conducive
GL88	- 1800	n9; 1734	Conducive
GL89	- 2057	none	Dismissed – no image
GL90	-2344	n11; 2320	Dismissed – no data
GL91	29Jun – 0249	n10; 0221	Conducive
GL92	- 0547	29Jun; n9; 0458	Conducive
GL93	- 0841	none	Dismissed – no image
GL94	- 1645	n9; 1721	Conducive

APPENDIX B. FORMULAE AND PROCEDURES

The following description of the formulae and procedures used in processing the sounding data from the MAST experiment was provided by William Syrett of Pennsylvania State University.

The measured parameters were pressure, temperature and relative humidity, with winds calculated using the Omega network. The "Omega" winds were averaged over a four-minute period by the sounding system software. Raw temperature and humidity data were output at 1.5 second intervals, with winds output every 10 seconds. The raw temperatures and humidities were cleaned up and then averaged to 5-second intervals, while winds were simply interpolated to 5 seconds.

Derived quantities include height, dewpoint and mixing ratio. The formulas and procedures used for mixing ratio, dewpoint and height are (in FORTRAN format):

Mixing Ratio (w):

w = 622.0*(e/(p-e)) p = pressure (mb)
e = vapor pressure (mb)

where: e = RH*es/100.0 RH= relative humidity
es= sat. vapor pres. (mb)

where: es= 6.112*EXP((17.67*T)/(T+243.5))
T = temperature (deg C)

Height (z):

z(i) = z(i-1)+(R*TvA/g)*LN(p(i-1)/p(i)) R = gas constant (J/kg K)
g = acc. due to gravity

where: TvA is the layer-averaged virtual temp;

Tv = T*(1.0+0.61*w) ; w in g/g, Tv in degrees Kelvin for height computation.

Dewpoint:

Td = (243.5*LN(e/6.112))/(17.67-LN(e/6.112))

Please note that the relative humidities were adjusted upward, based on both observed cloudiness in relation to reported humidities and also on a conversation with a Vaisala employee familiar with the humidity sensor on the RS-80 sondes used at the sites. The adjustment procedure is similar to that used for ASTEX soundings, except the maximum upward adjustment has been increased to 7%, up from 5%. The adjustment procedure is described next.

*** Upward Adjustment of Relative Humidity Values ***

An initial data quality check was run. A maximum value was determined from the accepted relative humidities. If the maximum unadjusted humidity was greater than or equal to 65% a correction factor was added to the maximum humidity. This factor ranges from 1% if the maximum unadjusted humidity was 65%, to 7% if the highest humidity was 93%. Maxima at or above 93% were adjusted to 100%.

This correction factor (C.F.) was then linearly weighted according to the humidity. The equation for humidity adjustment is:

RH(new) = RH(old) + ((RH(old) - 20.0)/(RH(max) - 20.0)) * C.F.

There was no adjustment if the humidity was less than 20%.

Obvious, singular bad data (spikes in humidity and temperature) were removed. Unstable lapse rates found in the lowest layers were the result of insufficient exposure of the sonde to the ambient environment before launch (primarily early in the campaign) and

were thus removed. If the surface temperature had to be lowered more than 0.5 degrees Celsius a comment was generated in the summary table. Only the lowest levels were adjusted as by 20 seconds into launch the temperature sensor generally had "caught up" with the actual (generally dry-adiabatic) profile.

The general data quality was quite good. Temperature data were consistently of high quality with the exception of the false super-adiabatic layers. Humidity data were generally of good quality, although values were a few percent low when the air was moist. The humidity profiles for several of the first approximately 35 soundings appeared "unrealistic" in real time. The problem, if it is one, manifested itself as regions of higher relative humidity just above the inversion. The resulting mixing ratio profiles appeared unrealistic. Specifically, soundings 10, 11, 23, 32, 33 and 34 are suspect- use with CAUTION!

Note: Soundings 10, 11, 23, 32, 33, and 34 were analyzed more closely and soundings 32 and 33 were deemed useful for the purposes of this study.

Low-level winds were unfortunately difficult to obtain. It was often difficult to get a "lock", necessary for low-level winds, while the sonde was on board. Winds generally began being received when the sonde was above 1 km in altitude.

THIS PAGE INTENTIONALLY LEFT BLANK

LIST OF REFRENCES

Brenner, J.R., 1994: Continental Aerosol Effects on Stratocumulus Microphysics During MAST 1994, M.S. Thesis, Naval Postgraduate School, Monterey, CA, 60pp.

Eloranta, E.E., J.M. King and J.A. Weinman, 1975: The determination of wind speed in the boundary layer by monostatic lidar. *Journal of Applied Meteorology*, **14**, 1485 - 1489.

Davidson, K.L., 2000: Personal conversation between K.L. Davidson Professor Naval Postgraduate School, Monterey, CA, and the author, 15 May 2000

Durkee, P. A., K. J. Noone and R. T. Bluth, 2000: The Monterey Area Ship Track (MAST) Experiment. *J. Atmos. Sci.,* In press.

Gaynor, J.E., and P.A. Mandics, 1978: Analysis of the tropical marine boundary layer during GATE using acoustic sounder data. *Monthly Weather Review*, **106**, 223 – 232.

Hasler, A.F., Strong, J., Woodward, R.H., and Pierce, H. (1991), Automatic analysis of stereoscopic satellite image pairs for determination of cloud-top height and structure. *J. Appl. Meteorol.* **30**, 257-281.

Hsieh, W., "Atmospheric Convection", [http://www.science.ubc.ca/~ocgy308/chap9/ch9_c.html], Aug 1997

Kidder, S.Q., and Vonder Haar, T.H., 1995: *Satellite Meteorology an Introduction.* Academic Press, San Diego. 466pp.

Klein, S.A., and Hartmann, D.L., 1993: The seasonal cycle of low stratiform clouds. *J. Climate*, **8**, 1587-1606.

Kren, J.R., 1987: Estimation of Marine Boundary Layer Depth and Relative Humidity with Multispectral Satellite Measurements. M.S. Thesis, Naval Postgraduate School, Monterey, CA, 73pp.

Kuze, A., and Chance, K.V., 1994: Analysis of cloud top height and cloud coverage from satellites using the O_2A and B bands. *J. Geophys. Res.* 99:14, 481-14, 492.

Ortenburger, L.N., Lawson, S.B., Patterson, B.J., 1985: Radiosonde Data Analysis I, Western Division GTE Government Systems Corporation, 1985.

Rogers, L.T., 1999: "Refractivity from clutter (RFC)," Presentation presented at the Naval Research Laboratory, Monterey, CA, 4 February 1999.

Rosenthal, J., Helvey, R., Battalino, T., Eddinton, L., Fisk, C., and Greiman, P., Predicting the EM/EO Environment from Satellite, Synoptic and In-Situ Data Sources, *Proceedings: Electromagnetic/Electro-Optics Prediction Requirements & Products Symposium.* pp73-86, 1997

Rosenthal, J.S., 2000: Personal conversation between J.S. Rosenthal Naval Warfare Center, Point Mugu, CA, and the author, 13 June 2000

Shenk, W.E., Holub, R.J., and Neff, R.A. (1975), Stereographic cloud analysis from a Apollo photographs over a cold front. *Bull. Am. Meteorol.* Soc. **56**, 4-16.

Simpson, J.J., McIntire, T., Zhonghai, J., Stitt, J.R., 2000: Improved cloud top height retrieval under arbitrary viewing and illumination conditions using AVHRR data. *Remote Sensing of Environment*, **72**, 95-110.

Stull, R.B., 1988: *An Introduction to Boundary Layer Meteorology*. Kluwer Academic Publishers, Dordrecht. 666pp.

Tjernström, M., "Marine Stratocumulus" [http://www.met.uu.se/eng/forsk/marine.html], Feb 1998

Trehubenko, E.J., 1994: Shiptracks in the Californian Stratus Region: Dependency on Marine Atmospheric Boundary Layer Depth. M.S. Thesis, Naval Postgraduate School, Monterey, CA, 88pp.

INITIAL DISTRIBUTION LIST

1. Defense Technical Information Center 2
   8725 John J. Kingman Road, Suite 0944
   Ft. Belvoir, VA 22060-6218

2. Dudley Knox Library 2
   Naval Postgraduate School
   411 Dyer Road
   Monterey, CA 93943-5101

3. Marvin B. McBride III 2
   1200 Greenbriar Ln.
   Arlington, TX 76013

4. Professor Philip Durkee 2
   Department of Meteorology (Code MR/De)
   Naval Postgraduate School
   Monterey, CA 93943-5101

5. Professor Carlyle H. Wash 2
   Department of Meteorology (Code MR/Wx)
   Naval Postgraduate School
   Monterey, CA 93943-5101

6. Mary Jordan 1
   Department of Meteorology (Code MR/Jr)
   Naval Postgraduate School
   Monterey, CA 93943-5101

7. Jay S. Rosenthal 1
   Geophysics Branch (Code 521400E)
   Naval Air Warfare Center
   Point Mugu, CA 93042

8. Roger A. Helvey 1
   Geophysics Branch (Code 521400E)
   Naval Air Warfare Center
   Point Mugu, CA 93042